

THE PROGENITORS OF LOCAL ULTRA-MASSIVE GALAXIES ACROSS COSMIC TIME: FROM DUSTY STAR-BURSTING TO QUIESCENT STELLAR POPULATIONS

DANILO MARCHESINI¹, ADAM MUZZIN², MAURO STEFANON³, MARIJN FRANX², GABRIEL G. BRAMMER⁴, CEMILE Z. MARSAN¹,
BENEDETTA VULCANI⁵, J. P. U. FYNBO⁶, BO MILVANG-JENSEN⁶, JAMES S. DUNLOP⁷, FERNANDO BUITRAGO⁷

Accepted in the Astrophysical Journal

ABSTRACT

Using the UltraVISTA catalogs, we investigate the evolution in the 11.4 Gyr since $z = 3$ of the progenitors of local ultra-massive galaxies ($\log(M_{\text{star}}/M_{\odot}) \approx 11.8$; UMGs), providing a complete and consistent picture of how the most massive galaxies at $z = 0$ have assembled. By selecting the progenitors with a semi-empirical approach using abundance matching, we infer a growth in stellar mass of $0.56^{+0.35}_{-0.25}$ dex, $0.45^{+0.16}_{-0.20}$ dex, and $0.27^{+0.08}_{-0.12}$ dex from $z = 3$, $z = 2$, and $z = 1$, respectively, to $z = 0$. At $z < 1$, the progenitors of UMGs constitute a homogeneous population of only quiescent galaxies with old stellar populations. At $z > 1$, the contribution from star-forming galaxies progressively increases, with the progenitors at $2 < z < 3$ being dominated by massive ($M_{\text{star}} \approx 2 \times 10^{11} M_{\odot}$), dusty ($A_V \sim 1\text{--}2.2$ mag), star-forming ($\text{SFR} \sim 100\text{--}400 M_{\odot} \text{ yr}^{-1}$) galaxies with a large range in stellar ages. At $z = 2.75$, $\sim 15\%$ of the progenitors are quiescent, with properties typical of post-starburst galaxies with little dust extinction and strong Balmer break, and showing a large scatter in color. Our findings indicate that at least half of the stellar content of local UMGs was assembled at $z > 1$, whereas the remaining was assembled via merging from $z \sim 1$ to the present. Most of the quenching of the star-forming progenitors happened between $z = 2.75$ and $z = 1.25$, in good agreement with the typical formation redshift and scatter in age of $z = 0$ UMGs as derived from their fossil records. The progenitors of local UMGs, including the star-forming ones, never lived on the blue cloud since $z = 3$. We propose an alternative path for the formation of local UMGs that refines previously proposed pictures and that is fully consistent with our findings.

Subject headings: galaxies: evolution — galaxies: formation — galaxies: fundamental parameters — galaxies: high-redshift — galaxies: luminosity function, mass function — galaxies: stellar content

1. INTRODUCTION

One of the most controversial questions regarding the formation and evolution of galaxies is when and how today's most massive galaxies formed. In the standard paradigm of structure formation, dark matter halos build in a hierarchical fashion through the dissipationless mechanism of gravitational instability, while galaxies form inside these structures following the radiative cooling of baryons, with stars forming out of gas that cools within the halos. In this picture, the most massive galaxies are naturally at the endpoint of the hierarchical merging process, and offer an opportunity to constrain models of galaxy formation and evolution, since their predicted galaxy properties are sensitive to various model assumptions, such as gas cooling, star formation, stellar and AGN feedback processes, chemical evolution, and mergers (e.g., Baugh 2006; De Lucia et al. 2006; Henriques et al. 2012; and references therein).

In the local universe ($z \sim 0$), the most massive galaxies (i.e., stellar mass $M_{\text{star}} > 5 \times 10^{11} M_{\odot}$) constitute a homo-

geneous population. These local ultra-massive galaxies tend to live in high-density environments (typically rich groups or clusters of galaxies; e.g., Blanton et al. 2009 for a review) and are characterized by early-type morphologies, red rest-frame optical colors, extremely quiescent stellar populations, old mean stellar ages, significant enhancements of the α/Fe element ratio, and little dust attenuation, and populate the extreme massive end of the very tight red sequence (e.g., Bower et al. 1992; Kauffmann et al. 2003a; Kauffmann et al. 2004; Gallazzi et al. 2005; Nelan et al. 2005; Thomas et al. 2005; Baldry et al. 2006; Gallazzi et al. 2006; Thomas et al. 2010). In particular, two decades of archeological studies (i.e., the detailed investigation of the stellar populations in local galaxies to constrain their formations and evolutions with cosmic time) have robustly shown that the more massive the galaxy is today, the earlier its star formation must have started and more promptly must have subsided, in an apparently “anti-hierarchical” fashion of the star formation. Quantitatively, most of the stars in local ultra-massive galaxies must have formed in the first ~ 3 Gyr of cosmic history (i.e., $z > 2$) through short (< 1 Gyr, as low as ~ 0.2 Gyr for the most massive galaxies), hence intense, bursts of star formation (e.g., Renzini 2006; van Dokkum & van der Marel 2007; Thomas et al. 2010).

Increasingly more sophisticated models of galaxy formation and evolution have shown that the apparent down-sizing in the star formation of ultra-massive galaxies is not in contradiction with the hierarchical paradigm. Recent models do predict ‘anti-hierarchical’ star-formation histories for the most massive galaxies in a Λ CDM universe (with most stars formed by $z \sim 3$), whereas the assembly of these galaxies is indeed hierarchical, with $\sim 80\%$ of the final mass typically locked up in

¹ Department of Physics and Astronomy, Tufts University, Medford, MA 02155, USA

² Leiden Observatory, Leiden University, PO Box 9513, NL-2300 RA Leiden, The Netherlands

³ Physics and Astronomy Department, University of Missouri, Columbia, MO 65211, USA

⁴ Space Telescope Science Institute, 3700 San Martin Drive, Baltimore, MD 21218, USA

⁵ Kavli Institute for the Physics and Mathematics of the Universe (WPI), Todai Institutes for Advanced Study, University of Tokyo, Kashiwa 277-8582, Japan

⁶ Dark Cosmology Centre, Niels Bohr Institute, University of Copenhagen, Juliane Maries Vej 30, DK-2100 Copenhagen, Denmark

⁷ SUPA, Institute for Astronomy, University of Edinburgh, Royal Observatory, Edinburgh EH9 3HJ, UK

a single galaxy only at $z < 0.4$ and with a number of effective progenitors as high as ~ 5 for the most massive galaxies (e.g., De Lucia et al. 2006; De Lucia & Blaizot 2007).

These predictions are qualitatively in agreement with the nearly constant rest-frame optical luminosity density of red-sequence galaxies since $z \sim 1$ found by the COMBO-17 and the DEEP2 surveys (Bell et al. 2004; Faber et al. 2007). This result in fact implies that the stellar mass density in red-sequence galaxies has roughly doubled since $z \sim 1$ driven by a combination of galaxy merging and truncation of star formation of the blue star-forming population. In particular, Faber et al. (2007) have used these results in support of a scenario for the formation of massive red-sequence (spheroidal) galaxies involving early mass assembly and star formation (with such progenitors living on the blue cloud), followed by quenching (which migrates the progenitors onto the red sequence) and further dry merging (allowing for additional growth along the red sequence to explain the assembly of the most massive galaxies in the local universe).

However, an independent analysis by Cimatti et al. (2006) of the evolution of the rest-frame optical luminosity function of red-sequence galaxies since $z \sim 0.8$ from COMBO-17 and DEEP2 has shown that the massive ($M_{\text{star}} > 10^{11} M_{\odot}$) red-sequence galaxies have actually not grown in mass over the past ~ 7 billion years, while the inferred growth by a factor of ~ 2 of the stellar mass density of red-sequence galaxies since $z \sim 0.8$ appears due to the build-up of the less-massive red-sequence population. In addition to the anti-hierarchical formation of the stars, this result implies also an anti-hierarchical assembly of the stellar content of the most massive galaxies, in contrast to the predictions from theoretical models.

Recent measurements of the stellar mass function of galaxies out to redshift $z = 4$ have intensified the tension between observations and theoretical predictions. Indeed, increasingly wider and deeper near-infrared surveys have provided evidence for the existence of very massive galaxies (i.e., $\log(M_{\text{star}}/M_{\odot}) \gtrsim 11.5$) when the universe was only 1.5 Gyr old (i.e., $z \sim 4$), and of their number densities evolving very little in the following ~ 3 – 4 Gyr from $z = 4$ to $z \sim 1$ – 1.5 (e.g., Pérez-González et al. 2008; Marchesini et al. 2009; Marchesini et al. 2010; Brammer et al. 2011; Muzzin et al. 2013b; and references therein).

While the stellar mass function of galaxies provides a mean to measure the abundance of a galaxy population at a given time and the overall growth as a function of time of its stellar content, it does not tell us how individual galaxies have evolved and assembled their mass. Ultimately, we would like to be able to connect local ultra-massive galaxies with their progenitors in the early universe to understand how their stellar populations have actually changed over cosmic time and to answer the following outstanding questions. Do local ultra-massive galaxies really form in short and intense bursts of star formation at high redshift? When do they actually stop forming stars? How does their stellar population age? How much mass is assembled over time? Do they really evolve from the blue cloud to the red sequence as suggested by, e.g., Faber et al. (2007)?

Needless to say, answering these questions have proved difficult, as it requires the non-trivial task of linking galaxies and their descendants/progenitors through cosmic time, which in turn requires assumptions for how galaxies evolve. However, in recent years, several approaches have been developed to link galaxies across cosmic time. A popular approach easy to implement is to compare

galaxy properties at fixed cumulative number density (e.g., Wake et al. 2006; Tojeiro & Percival 2010; Brammer et al. 2011; Papovich et al. 2011; Tojeiro et al. 2012; Patel et al. 2013; van Dokkum et al. 2013; Leja et al. 2013; Muzzin et al. 2013b). While this approach has the advantage of relying solely on observations, it does not take into account galaxy-galaxy mergers and scatter in mass accretion histories, both affecting the median cumulative number density of a galaxy population (Leja et al. 2013; Lin et al. 2013; Behroozi et al. 2013a). More advanced comparisons have adopted either semi-analytical or semi-empirical galaxy-halo connections to deduce galaxy evolution from simulated dark matter merger histories (e.g., Conroy & Wechsler, 2009; Leitner 2012; Behroozi et al. 2013a; Moster et al. 2013; Wang et al. 2013; Lu et al. 2012; Leja et al. 2013; Lin et al. 2013; Mutch et al. 2013; Lu et al. 2014; Behroozi et al. 2013b; and references therein).

In this paper, we investigate the evolution with cosmic time of the progenitors of local ultra-massive ($M_{\text{star}} \approx 6 \times 10^{11} M_{\odot}$) galaxies from $z = 3$. The progenitors are selected using both the fixed cumulative number density technique and a semi-empirical approach using abundance matching in the Λ CDM paradigm. The stellar population properties of the progenitors are then studied as a function of redshift. This analysis provides a direct test of the star-formation histories predicted from the archeology studies of local ultra-massive galaxies and returns a clear and consistent picture of their evolution in the past 11.4 billion years of cosmic history.

Our paper is structured as follows: The adopted dataset and the selection of the sample of progenitors are described in §2 and §3, respectively. The evolution of the properties of the progenitors of local ultra-massive galaxies is presented in §4, while the results are summarized and discussed in §5. We assume $\Omega_M = 0.3$, $\Omega_{\Lambda} = 0.7$, and $H_0 = 70 \text{ km s}^{-1} \text{ Mpc}^{-1}$. A Kroupa (2001) initial mass function (IMF) is assumed throughout the paper. All magnitudes are in the AB system.

2. THE DATASET

This study uses the K_S -selected catalog of the COSMOS/UltraVISTA field from Muzzin et al. (2013a). The catalog includes PSF-matched photometry in 30 photometric bands over the wavelength range $0.15 \mu\text{m} \rightarrow 24 \mu\text{m}$ from the available GALEX (Martin et al. 2005), CFHT/Subaru (Capak et al. 2007), UltraVISTA (McCracken et al. 2012), and S-COSMOS (Sanders et al. 2007) datasets. Sources are selected from the DR1 UltraVISTA K_S -band imaging (McCracken et al. 2012) which reaches a depth of $K_{S,\text{tot}} < 23.4$ at 90% completeness. A detailed description of the photometric catalog construction, photometric redshift measurements, and stellar population properties' estimates (e.g., stellar mass) is presented in Muzzin et al. (2013a), which accompanies the public release of all data products from the catalog. A brief description of the relevant aspects of the catalog with respect to our analysis is also provided in Muzzin et al. (2013b), presenting the measurements of the stellar mass function of galaxies, including quiescent and star-forming galaxies, from $z = 4$ to $z = 0.2$.

Briefly, stellar population properties were derived by fitting the observed spectral energy distributions (SEDs) from the GALEX UV to the *Spitzer*-IRAC $8 \mu\text{m}$ photometry with Bruzual & Charlot (2003) models assuming exponentially-declining star-formation histories (SFHs) of the form $\text{SFR} \propto e^{-t/\tau}$, where SFR is the star formation rate, t is the time since the onset of star formation, and τ sets the timescale of the de-

cline in the SFR, solar metallicity, a Calzetti et al. (2000) dust law, and a Kroupa (2001) IMF. We allow $\log(\tau/\text{Gyr})$ to range between 7.0 and 10.0 Gyr, $\log(t/\text{Gyr})$ between 7.0 and 10.1 Gyr, and A_V between 0 and 4 mag. Median random errors on stellar mass, SFR, stellar age, and dust extinction are $^{+0.05}_{-0.09}$ dex, ± 0.2 dex, $^{+0.1}_{-0.2}$ dex, and $^{+0.3}_{-0.2}$ mag, respectively, for the quiescent progenitors, and $^{+0.09}_{-0.18}$ dex, ± 0.6 dex, $^{+0.2}_{-0.4}$ dex, and $^{+0.6}_{-0.4}$ mag, respectively, for the star-forming progenitors, similar to the typical uncertainties from low-resolution spectroscopy (Muzzin et al. 2009). To assess the systematic effects of the adopted SED-modeling assumptions, we have also investigated different SFHs, metallicities, and extinction curves (see §4.6.3).

The SFRs from SED modeling can be strongly influenced by the assumption of the SFH. A more robust estimate of the instantaneous SFR is obtained from the combination of the rest-frame UV flux (L_{2800}) and the rest-frame total infrared luminosity (L_{IR}). To determine L_{2800} we used EAZY (Brammer et al. 2008) to integrate the best-fit template over the wavelength range 2600-2950Å. The inclusion of the *GALEX* photometry in the UltraVISTA multi-wavelength catalogs of Muzzin et al. (2013a) guarantees that L_{2800} is constrained by the data over the full targeted redshift range. The approach presented in Wuyts et al. (2008) was followed to determine L_{IR} from the $24\mu\text{m}$ emission. Specifically, as already described in detail in Marchesini et al. (2010), we used the infrared SEDs of star-forming galaxies from Dale & Helou (2002), which allow us to derive the IR/MIR flux ratio for different heating levels of the interstellar environment, parameterized by $dM(U) \sim U^{-\alpha} dU$, where $M(U)$ is the dust mass heated by an intensity U of the interstellar field. The total infrared luminosity $L_{\text{IR},\alpha}$ was computed for each template in Dale & Helou (2002) within the range $1 \leq \alpha \leq 2.5$. We adopted the log-average of the resulting $L_{\text{IR},\alpha=1,\dots,2.5}$ as the best estimate for the IR luminosity. This approach returns SFRs in better agreement with the SFRs estimated from SED modeling (Franx et al. 2008; Wuyts et al. 2008) and from dust-corrected $\text{H}\alpha$ line fluxes (Muzzin et al. 2010), compared to the often adopted local luminosity-dependent approaches, which systematically overestimate SFRs by a factor of 4-6 (e.g., Papovich et al. 2007; Murphy et al. 2009; Elbaz et al. 2010; Muzzin et al. 2010). We convert the L_{2800} into $\text{SFR}_{\text{UV,uncorr}}$ using the conversion factor $\text{SFR}_{\text{UV,uncorr}} = 3.234 \times 10^{-10} L_{2800}$ from Kennicutt (1998), adapted to a Kroupa (2001) IMF by Bell et al. (2005). $\text{SFR}_{\text{UV,uncorr}}$ is the observed SFR, and is not corrected for dust extinction. The L_{IR} is converted into a SFR_{IR} using $\text{SFR}_{\text{IR}} = 0.98 \times 10^{-10} L_{\text{IR}}$ from Kennicutt (1998), adapted to a Kroupa (2001) IMF. The total SFR of the galaxies is then derived via $\text{SFR}_{\text{tot}} = \text{SFR}_{\text{UV,uncorr}} + \text{SFR}_{\text{IR}}$.

3. SELECTION OF THE PROGENITORS OF LOCAL ULTRA-MASSIVE GALAXIES

3.1. Fixed Cumulative Number Density

Following previous studies (e.g., Wake et al. 2006; Tojeiro & Percival 2010; Brammer et al. 2011; Papovich et al. 2011; Tojeiro et al. 2012; Patel et al. 2013; van Dokkum et al. 2013; Leja et al. 2013; Muzzin et al. 2013b), we connect progenitor galaxies by requiring that they have the same cumulative co-moving number density of the low-redshift galaxy population, i.e., galaxies at $0.2 < z < 0.5$ with $M_{\text{star}} \approx 5 \times 10^{11} M_{\odot}$. Effectively, galaxies are ranked according to their stellar mass and we select galaxies at

different redshifts that have the same rank order as the low-redshift population. The implicit assumption is that rank order is conserved through cosmic time, or that processes that break the rank order do not have a strong effect on the average measured properties.

In order to apply the fixed cumulative number density selection, we derive cumulative number densities, $n(> M_{\text{star}})$, as a function of stellar mass using the recently published and publicly available stellar mass functions from the UltraVISTA survey (Muzzin et al. 2013b). The contributions from Poisson errors, cosmic variance, and photometric redshift uncertainties to the total error budget of the stellar mass functions were quantified and presented in Muzzin et al. (2013b). We refer to this paper for a detailed description of the derivations of the errors of the stellar mass functions. The left panel of Figure 1 shows $n(> M_{\text{star}})$ in the six targeted redshift ranges from $z = 0.2$ to $z = 3.0$, namely $0.2 \leq z < 0.5$, $0.5 \leq z < 1.0$, $1.0 \leq z < 1.5$, $1.5 \leq z < 2.0$, $2.0 \leq z < 2.5$, $2.5 \leq z < 3.0$. Also shown is the total 1σ error (including Poisson errors, cosmic variance, and photometric redshift uncertainties) on $n(> M_{\text{star}})$ for the lowest and highest targeted redshift bins. Galaxies with stellar masses $M_{\text{star}} \approx 5 \times 10^{11} M_{\odot} = 10^{11.7} M_{\odot}$ at $z = 0.35$ have a cumulative number density of $3 \times 10^{-6} \text{Mpc}^{-3}$ (shown by the horizontal dashed line in the left panel of Fig. 1). We then trace the progenitors of these galaxies by identifying, at each redshift, the stellar mass for which the cumulative number density is $3 \times 10^{-6} \text{Mpc}^{-3}$ (indicated in the left panel of Fig. 1 by the filled triangles).

The stellar mass evolution for galaxies with the rank order of the low- z population is shown in the right panel of Figure 1 with colored filled triangles. Also shown is the formal 1σ uncertainty on the stellar mass of the progenitors at the given cumulative number density and including the contributions from Poisson errors, cosmic variance, and photometric redshift uncertainties. As previously done in the literature (e.g., van Dokkum et al. 2013), we parameterize the evolution of the stellar mass of the progenitors with a quadratic function of the form $\log(M_{\text{progen}}(z)/M_{\odot}) = A + Bz + Cz^2$, with $A = 11.796 \pm 0.043$, $B = -0.291 \pm 0.076$, and $C = 0.060 \pm 0.028$ (dashed curve in the right panel of Fig. 1), corresponding to a value of the stellar mass in the local universe of $\log(M_{\text{progen}}(z=0)/M_{\odot}) = 11.8$. This value is comparable to the typical stellar masses of local brightest cluster galaxies (BCGs; e.g., Lidman et al. 2012; Lin et al. 2013).

3.2. Semi-empirical Approach Using Abundance Matching

The fixed cumulative number density approach does not take into account galaxy-galaxy mergers and scatter in mass accretion histories, both altering the median cumulative number density of a galaxy population (Leja et al. 2013; Lin et al. 2013; Behroozi et al. 2013a). Therefore, to select the progenitors we also adopt a semi-empirical approach using abundance matching in the ΛCDM paradigm, accounting for mergers and scatter in mass accretion histories. A detailed description of this technique is presented in Behroozi et al. (2013b) (and references therein), who also made publicly available the code implementing this technique.⁸ Briefly, the galaxy cumulative number density at redshift z_1 is converted to a halo mass with equal cumulative number density using peak halo mass functions. Then, for halos at that mass at z_1 , the masses of the most-massive progenitor halos at $z_2 > z_1$ are recorded using to the halos' mass accretion histories. Finally, the median

⁸ <http://code.google.com/p/nd-redshift/>

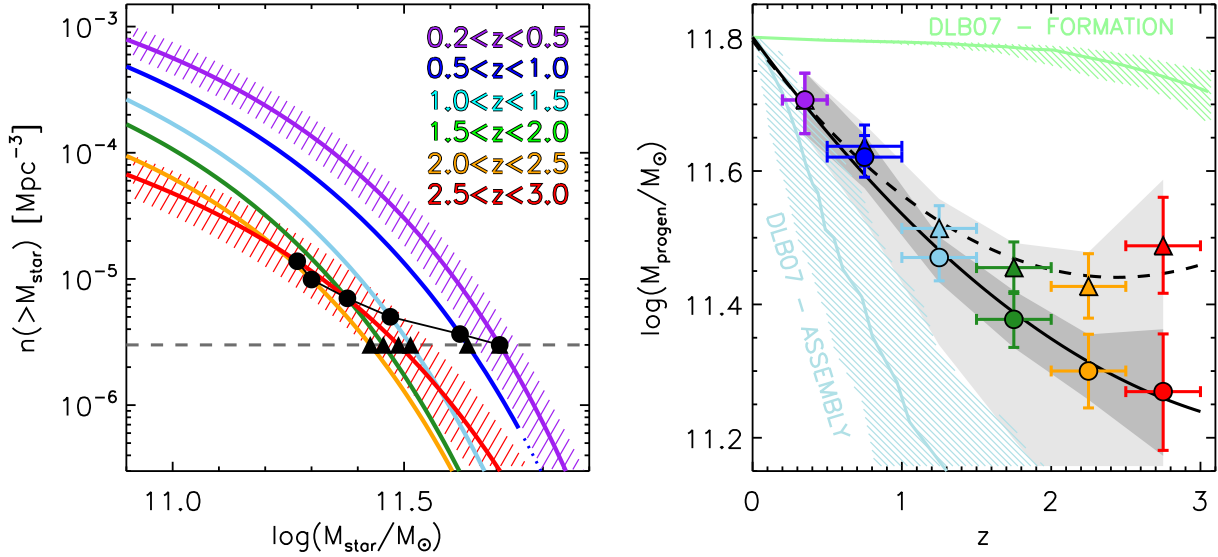


FIG. 1.— **Left panel:** Cumulative number density, $n(> M_{\text{star}})$, as a function of stellar mass obtained by integrating the stellar mass functions from the UltraVISTA survey (Muzzin et al. 2013b) at $0.2 < z < 3.0$. The different colors correspond to the different targeted redshift intervals. Filled triangles show the evolution in stellar mass for galaxies at fixed cumulative number densities of $3 \times 10^{-6} \text{ Mpc}^{-3}$, shown by the dashed horizontal gray line. Filled circles show evolution in stellar mass after inclusion of the evolving number density for galaxy progenitors using an abundance matching approach (§3.2). The hatched regions show the 1σ range of $n(> M_{\text{star}})$ including Poisson errors, cosmic variance, and photometric redshift uncertainties. The 1σ range of $n(> M_{\text{star}})$ is plotted only for the lowest and highest targeted redshift intervals for clarity. **Right panel:** Evolution of the stellar mass of the progenitors, M_{progen} , as a function of redshift. Filled triangles are obtained using the fixed cumulative number density approach, whereas filled circles are derived using the semi-empirical approach using abundance matching. The error bars show the width of the redshift bin and the formal 1σ uncertainty in stellar mass at a given cumulative number density and includes Poisson errors, cosmic variance, and photometric redshift uncertainties. The black dashed and solid curves show the evolutions of the stellar mass as a function of redshift (parameterized as $\log(M_{\text{star}}) = A + Bz + Cz^2$) derived from the constant cumulative number density and abundance matching approaches, respectively. The progenitors of $z \sim 0$ UMGs (i.e., $\log(M_{\text{star}}/M_{\odot}) = 11.8$) are selected in a narrow range of stellar mass around these curves. The dark gray filled region shows the 1σ uncertainty on the stellar mass growth of the progenitors as selected using the abundance matching approach when only the errors on the observed stellar mass functions are considered. The light gray filled region shows instead the 68th-percentile range in stellar mass including both the errors on the observed stellar mass functions and the spread from individual galaxy growth histories. Specifically, the 68-th percentile range was estimated by generating 1000 realizations of the stellar mass tracks from 1000 realizations of the stellar mass functions and of the galaxy accretion histories (Behroozi et al. 2013b). The color curve and hatched region represent the median and the 15th/85th percentile range, respectively, of the assembly history (light blue) and the star-formation history (light green) of BCGs as simulated in De Lucia & Blaizot (2007).

halo progenitor mass at z_2 is converted back into cumulative number densities using the halo mass function at z_2 .

Similarly to the fixed cumulative number density approach, the progenitors of the low- z population of very massive galaxies are traced by identifying, at each redshift, the stellar mass for which the evolving cumulative number density (determined with the semi-empirical approach using abundance matching) intersects the cumulative number density curves derived from the UltraVISTA stellar mass functions (plotted as filled circles in the left panel Fig. 1).

The resulting stellar mass evolution with the corresponding 1σ uncertainty is shown in the right panel of Figure 1 with colored filled circles. Errors on the stellar mass of the progenitors were derived in the same way as described in §3.1. Adopting the same parameterization as for the fixed cumulative number density approach, we find $A = 11.801 \pm 0.038$, $B = -0.304 \pm 0.054$, and $C = 0.039 \pm 0.014$, also implying a value of the stellar mass in the local universe of $\log(M_{\text{progen}}(z=0)/M_{\odot}) = 11.8$ (continuous curve in the right panel of Fig. 1).

4. EVOLUTION OF THE PROGENITORS' PROPERTIES

Here we study and present the evolution as a function of cosmic time of the properties of the progenitors of local ultra-massive ($\log(M_{\text{star}}/M_{\odot}) = 11.8$) galaxies (UMGs, hereafter) since $z = 3$. For a given redshift, we select the progenitors of $z \sim 0$ UMGs within a bin of size ~ 0.2 dex in stellar mass centered on $M_{\text{progen}}(z)$, following the approach

adopted by Patel et al. (2013). The actual boundaries of the bins are adjusted such that the median mass is close to the value given by $M_{\text{progen}}(z)$. Given the steepness of the stellar mass function, in practice this results in selecting galaxies at $(\log M_{\text{progen}}(z)/M_{\odot})^{+0.15}_{-0.07}$.

4.1. Stellar Mass Evolution

As shown by the dashed curve in the right panel of Figure 1, the evolution in stellar mass of the progenitors of $z \sim 0$ UMGs is quite small when the progenitors are selected using the fixed cumulative number density method, i.e., 0.33 ± 0.15 dex (i.e., a factor of $\sim 2.1^{+1.0}_{-0.6}$) from $z = 3.0$ to $z = 0$. Therefore, about half of the stellar mass in local UMGs was assembled at $z > 3$, i.e., in the first 2 Gyr of cosmic history. If the progenitors are instead selected with the semi-empirical approach using abundance matching, the evolution in stellar mass is much more significant, 0.56 ± 0.21 dex, 0.45 ± 0.13 dex, and 0.27 ± 0.08 dex from $z = 3.0$, $z = 2.0$, and $z = 1.0$, respectively, to $z = 0$. Therefore, the progenitors have grown by a factor of $\sim 3.6^{+2.3}_{-1.4}$ over the last 11.4 Gyr from $z = 3.0$ to $z = 0$, with only about a fourth of the stellar mass in local UMGs having been assembled by $z \sim 3$. If the 68th-percentile range in stellar mass (shown in Figure 1 as a light gray filled region) resulting from the scatter in the progenitors' number density is included in the error budget, the uncertainty on the inferred growth would be larger by a factor up to ~ 1.7 , i.e., $0.56^{+0.35}_{-0.25}$ dex, $0.45^{+0.16}_{-0.20}$ dex, and $0.27^{+0.08}_{-0.12}$ dex from $z = 3.0$,

$z = 2.0$, and $z = 1.0$, respectively, to $z = 0$.

The right panel of Figure 1 also shows the predicted median and 15th/85th percentiles of the ‘formation’ (light blue) and ‘assembly’ (light green) histories of BCGs from the theoretical study using semi-analytic techniques presented in De Lucia & Blaizot (2007). The formation history of BCGs is defined as the sum of the stellar masses in all progenitors at each time, whereas their assembly history corresponds to the stellar mass of the main branch. As highlighted in De Lucia & Blaizot (2007), there is a very small scatter in the formation histories of BCGs, with most of their stars having formed at $z > 3$ ($\sim 90\%$ of the stars formed at $z > 2.5$). The assembly histories exhibit a much larger scatter with a much later assembly time. Specifically, the fraction of mass in the main progenitor varies between 15% and 40% at $z = 1$, and between 40% and 70% at $z = 0.5$ (De Lucia & Blaizot 2007). Figure 1 shows that the inferred evolutions in stellar mass of the progenitors of $z \sim 0$ UMGs (solid or dashed curves) are faster than the model-predicted assembly histories, but much slower than the predicted formation histories of BCGs. In other words, in semi-analytic models most of the stars were not formed in the main branch, but star formation happened very early in low- to intermediate-mass halos (with stellar masses \sim a few $\times 10^{10} M_{\odot}$), which were accreted steadily over time following the assembly history of the dark matter. We note that, as the median cumulative number density of the progenitors increases with redshift as $\sim (0.2\Delta z)$ (Behroozi et al. 2013b), using the fixed cumulative number density approach would preferentially select progenitors which potentially had an unusually rapid assembly at earlier times. This should be kept in mind in the comparison between the model-predicted assembly history of BCGs with the inferred growth in stellar mass of the progenitors of local UMGs selected with the fixed cumulative number density approach. At $z = 3$, the progenitors of UMGs have a typical observed stellar mass of $\log(M_{\text{star}}/M_{\odot}) \approx 11.2$, a factor of ~ 5 larger than the model-predicted stellar mass assembled by $z = 3$, implying a predicted abundance of BCGs’ progenitors at $z = 3$ significantly larger than observed. We note that the dominant source of uncertainty in the stellar mass evolution of the progenitors is due to the scatter in the progenitors’ cumulative number density. When this source of error is included, as shown by the light gray filled region in the right panel of Figure 1, the disagreement between the observed stellar growth of local UMGs and the model-predicted assembly history of BCGs becomes less significant, and the two marginally agree at the $\sim 2\sigma$ level.

The disagreement between observed and model-predicted evolutions of the stellar mass content of the progenitors of local UMGs is another manifestation of the previously highlighted tensions between observed and model-predicted stellar mass functions. Specifically, semi-analytic models were found to significantly overpredict the observed number density of galaxies below $10^{11} M_{\odot}$ at $z \gtrsim 1-1.5$ and to underpredict the number density of massive galaxies at $z > 2$ (e.g., Marchesini et al. 2009), with low-mass galaxies in the stellar mass range $10^9 - 10^{11} M_{\odot}$ forming too early in the models and being too passive at later times (e.g., Fontanot et al. 2009; see also Henriques et al. 2012). We note that, whereas the typical errors on stellar masses are not large enough to explain the disagreement at the high-mass end between the observed and the model-predicted stellar mass functions at $z \gtrsim 1$ (e.g., Ilbert et al. 2013), the disagreement between the inferred evolution in stellar mass of the progenitors of local UMGs and the model-predicted assembly history of BCGs shown in Fig-

ure 1 could potentially be further reduced (although at most only partly) if the model predictions were to be convolved by the typical statistical errors in the stellar masses of UltraVISTA.

Whereas the inferred growth in stellar mass from $z = 3$ is quite different depending on the adopted method to select the progenitors, the derived evolution in the stellar population parameters (e.g., rest-frame colors, level of star formation activity, stellar ages, extinction, rest-frame optical absolute magnitudes, and mass-to-light ratios) is qualitatively similar. Moreover, observationally, recent works have robustly revealed that most early-type galaxies show tidally disrupted features indicative of their past merging histories (e.g., Malin & Carter 1983; van Dokkum 2005; Tal et al. 2009; Janowiecki et al. 2010; Sheen et al. 2012), with evidence of major dry (i.e., dissipationless) merging being an increasingly important mechanism for the evolution of galaxies with $M_{\text{star}} > 10^{11.4} M_{\odot}$ (e.g., Kim & Im 2013). Contrary to the fixed cumulative number density method, the semi-empirical approach using abundance matching accounts for mergers, making the latter a more desirable approach to constrain the evolution of the median cumulative number density for a galaxy population (Behroozi et al. 2013b). Therefore, in the sections below, we present only the evolution of the stellar population properties of the progenitors of $z \sim 0$ UMGs when selected with the semi-empirical approach using abundance matching. For completeness, Appendix A presents the evolution of the stellar population properties of the progenitors of local UMGs when selected with the fixed cumulative number density method.

4.2. Evolution in Rest-frame $U - V$ and $V - J$ Colors

The rest-frame $U - V$ versus $V - J$ color-color diagram (hereafter the UVJ diagram) has become, in recent years, a common tool to separate quiescent from star-forming galaxies for its ability to separate red galaxies that are quiescent from reddened (i.e., dust obscured) star-forming galaxies (see, e.g., Labbé et al. 2006; Wuyts et al. 2007; Williams et al. 2009; Brammer et al. 2011; Patel et al. 2011; Whitaker et al. 2011; Muzzin et al. 2013b). Figure 2 shows the evolution of the rest-frame $U - V$ and $V - J$ colors of the progenitors of UMGs since $z = 3$ (colored filled circles), along with the evolution of the rest-frame $U - V$ and $V - J$ colors of the overall galaxy population (grayscale representation) above the 95% mass-completeness limit from the UltraVISTA survey. To distinguish between star-forming and quiescent galaxies we use the same box adopted in Muzzin et al. (2013b) for the study of the evolution of the stellar mass functions of star-forming and quiescent galaxies since $z = 4$. The adopted box is plotted in Figure 2, with the quiescent and star-forming progenitors highlighted in red and blue, respectively. Color evolution tracks from the stellar population synthesis models of Bruzual & Charlot (2003) are also plotted in Figure 2 for different assumed star-formation histories (SFHs) and amount of dust extinction: an exponentially declining SFH with an e-folding timescale of $\tau = 100$ Myr and no dust extinction (τ_{100} ; dark gray track), a constant SFH with no dust (CSF; light blue), and the same CSF model with $A_V = 2$ mag of extinction (light brown). The color tracks are plotted up to the maximum allowed age of the universe corresponding to the lower limit of each redshift interval. We note that the τ_{100} color track is very similar to the color track of a single stellar population, with the latter reaching the same $U - V$ and $V - J$ colors of the τ_{100} model at slightly younger (by ~ 0.2 Gyr) ages.

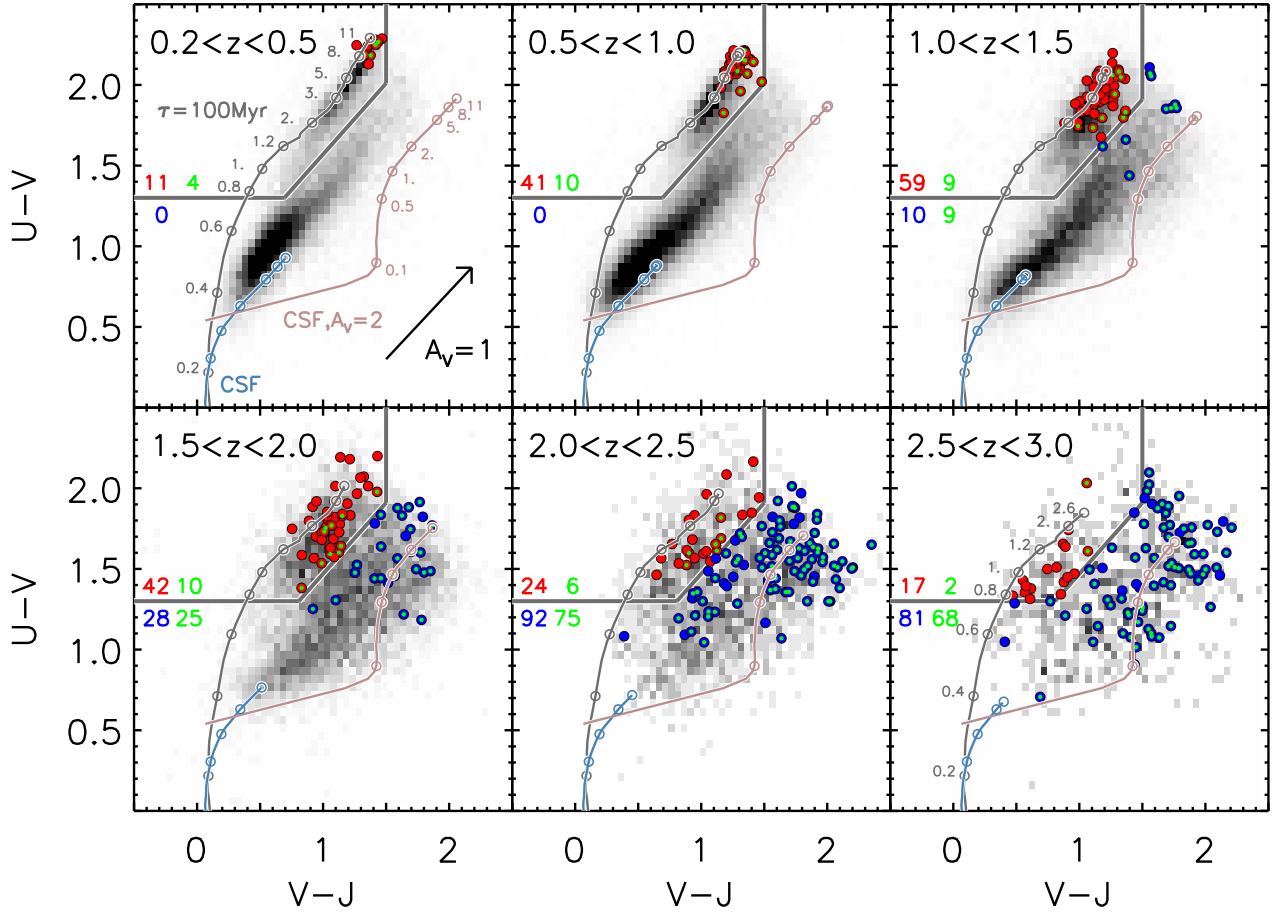


FIG. 2.— Rest-frame $U-V$ versus $V-J$ diagram in the targeted redshift intervals between $z = 0.2$ and $z = 3.0$ for the progenitors of local UMGs selected with the semi-empirical approach using abundance matching. The cuts used to separate star forming from quiescent galaxies from Muzzin et al. (2013b) are shown as the solid dark gray lines. Red and blue filled circles highlight the quiescent and star-forming galaxies among the progenitors' sample. Listed are the numbers of quiescent (red) and star-forming (blue) progenitors in each redshift interval. The grayscale representation of the overall galaxy population above the 95% mass-completeness limit from the UltraVISTA survey is also plotted in each redshift interval. Small green circles show the progenitors detected in the *Spitzer*-MIPS $24\mu\text{m}$ data with signal-to-noise $S/N > 5$. The numbers of MIPS-detected galaxies among the quiescent and star-forming progenitors are listed in green. Most of the star-forming galaxies are robustly detected in MIPS, whereas only a small fraction of quiescent galaxies is detected at $24\mu\text{m}$. Color evolution tracks of Bruzual & Charlot (2003) models are also shown: an exponentially declining SFH with no dust ($\tau=100$ Myr; dark gray), a constant SFH with no dust (CSF; light blue), and the same CSF model with $A_V = 2$ mag of extinction (light brown). The evolution tracks are plotted up to the maximum allowed age of the universe corresponding to the lower limit of each redshift interval. The empty circles represent the model colors at the specified ages (in Gyr). The dust vector indicates an extinction of $A_V = 1$ mag for a Calzetti et al. (2000) extinction curve. The population of progenitors of local UMGs shows a range in properties at $2.5 < z < 3.0$, typical of a heterogeneous population mostly dominated by dusty ($A_V = 1.5-2$ mag) star-forming galaxies, but also including post-starburst quiescent galaxies. By $z = 0.35$, such heterogeneous population has turned into a homogeneous population of maximally old, quiescent galaxies with very similar colors.

At $0.2 < z < 0.5$, the progenitors of UMGs constitute a homogeneous population with similar rest-frame $U-V$ and $V-J$ colors, typical of quiescent galaxies with old (age > 8 Gyr) stellar populations (from the comparison with the τ_{100} color track). As the progenitors of UMGs are followed to higher redshifts, such population becomes increasingly diversified. Out to $z = 1$, the progenitors are still all quiescent galaxies and constitute a homogeneous population, while at $z > 1$ the contribution from star-forming galaxies progressively increases, with the population of the progenitors being dominated by star-forming galaxies at $2 < z < 3$. Quantitatively, the fraction of quiescent galaxies in the progenitors of local UMGs is seen to decrease from 100% at $z \leq 1$, to $\sim 86\%$ at $z = 1.25$, and down to $\sim 17\%$ by $z = 2.75$.

The location of the star-forming progenitors in the UVJ diagram clearly indicates that these galaxies are quite dusty, with typical extinction in the visual band of $A_V \sim 1.5-2$ mag (inferred from the comparison with the color track of a CSF

model with $A_V = 2$ mag). The dusty nature of the star-forming progenitors can be further tested with *Spitzer*-MIPS $24\mu\text{m}$ data. For the targeted redshift range, the MIPS $24\mu\text{m}$ probes the rest-frame mid-infrared (MIR; ~ 6 and $20\mu\text{m}$ at $z = 3$ and $z = 0.2$, respectively), offering a powerful method of separating two basic SED types: evolved quiescent systems (whose stellar emission drops drastically at $\lambda_{\text{rest}} > 2\mu\text{m}$), and active dusty galaxies, i.e., those that are powered by either star formation or active galactic nuclei (AGNs), both of which produce substantial MIR emission (e.g., Webb et al. 2006). Specifically, in pure starburst galaxies, the MIR emission is dominated by features from polycyclic aromatic hydrocarbons (PAH) that are strong relative to the underlying dust continuum, which only begins to rise above $\sim 10\mu\text{m}$ (Draine & Li 2007). The hard radiation field of an AGN destroys PAH carriers, and the continuum emission from hot small dust grains is strong throughout the MIR (Genzel & Cesarsky 2000).

The progenitors of UMGs detected with a signal-to-noise ratio $S/N > 5$ in the MIPS $24\mu\text{m}$ data are shown in Figure 2 by green filled circles. On average, $\sim 84\%$ of the star-forming progenitors are robustly detected with $S/N > 5$ in MIPS, with a fraction of $24\mu\text{m}$ -detected sources as high as 90% at $z < 2$, supporting the dusty nature of the star-forming progenitors. We note that the adopted MIPS flux limit ($35\mu\text{Jy}$, 5σ) translates into a large range of MIR luminosities sampled at a broad range of rest-frame wavelengths over the large considered redshift range, preventing the detection rate alone to be an ideal proxy of the level of obscured star-formation activity as a function of redshift, since larger SFRs are needed in order to be detected at higher redshifts. Therefore, the roughly constant detection rate of the star-forming progenitors over the targeted redshift interval is a strong evidence for increasing levels of the dust-enshrouded activity with redshift in the star-forming progenitors of UMGs (see a more quantitative analysis of the evolution of the SFR and specific-SFR in §4.4.2).

In contrast to the star-forming progenitors, only $\sim 21\%$ of the quiescent progenitors are on average detected at $24\mu\text{m}$ with $S/N > 5$, with this fraction ranging from $\sim 36\%$ at $z = 0.35$ to $\sim 12\%$ at $z = 2.75$. This detection rate is quantitatively consistent with the MIPS detection rate found in a sample of quiescent galaxies at $0.3 < z < 2.5$ with $\log(M_{\text{star}}/M_{\odot}) > 10.3$ selected from the 3D-HST survey (Fumagalli et al. 2013). While the MIPS detection rate in the quiescent progenitors is a factor of ~ 4 smaller than in the star-forming progenitors, its not-zero value is potentially indicative of low levels of obscured star formation or AGN contamination. We see from Figure 2 that the MIPS detection in the quiescent progenitors have preferentially redder $V - J$ colors, lying closer to the line separating quiescent from dusty star-forming galaxies, suggesting the possibility of these galaxies being in their terminal phases of star formation and on their ways to become fully quenched systems. If these systems are indeed transitioning systems in their final approaches to the quiescent population, it is tempting to interpret their MIPS detections as potentially due to obscured AGNs responsible for the quenching of their star-formation activities, given the increasing fraction of AGN activity with increasing stellar mass found both in the local universe (e.g., Kauffmann et al. 2003b) and out to $z \sim 2.5$ (e.g., Papovich et al. 2006; Kriek et al. 2007). We note however that the investigation of the origin of the MIPS fluxes in the sample of quiescent, lower-mass galaxies in Fumagalli et al. (2013) appears to indicate that the low MIPS fluxes can be fully accounted by processes unrelated to obscured AGNs and on-going star formation, such as cirrus dust heated by old stellar populations and circumstellar dust embedding asymptotic giant branch stars. Related to the dust content, we finally note that the comparison in the UVJ diagram of the quiescent progenitors and the evolution tracks indicates an increasing amount of dust extinction with increasing redshift also in the quiescent progenitors of UMGs, especially at $z > 1 - 1.5$ (see also §4.4.3).

4.3. Evolution in the $U - V$ versus M_{star} diagram

As highlighted in the previous section, Figure 2 shows that the progenitors of UMGs at $z < 1$ constitute a homogeneous population, with very similar rest-frame $U - V$ and $V - J$ colors, typical of quiescent and old stellar populations. Two additional remarkable results are evident from Figure 2. First, the scatter in the rest-frame $U - V$ color of the quiescent progenitors becomes progressively larger with increasing redshift, especially at $z > 1.5$. Second, the star-forming progenitors

show similar rest-frame $U - V$ colors compared to the quiescent progenitors, indicative that the star-forming progenitors never lived on the blue cloud since $z = 3$. Even more remarkable is that a significant fraction of star-forming progenitors in the highest redshift bin show rest-frame $U - V$ colors redder than the quiescent progenitors, in addition to significantly redder rest-frame $V - J$ colors, suggesting that the star-forming progenitors at $z \sim 3$ of local UMGs may be actually redder than the quiescent progenitors.

These results can be better seen in Figure 3, which shows the rest-frame $U - V$ versus M_{star} diagram (or color-mass diagram; CMD, hereafter) of the quiescent and star-forming progenitors of UMGs. Figure 3 also shows the evolution in the CMD of the overall galaxy population (grayscale representation) from the UltraVISTA survey.

At $0.2 \leq z < 0.5$, the progenitors of local UMGs are the reddest objects and have similar rest-frame $U - V$ colors, with a very small intrinsic scatter (~ 0.04 mag). To measure the intrinsic scatter (σ_{int}), we corrected the observed scatter (σ_{obs}) for the scatter introduced by photometric errors (σ_{phot}) using the formula $(\sigma_{\text{obs}})^2 = (\sigma_{\text{int}})^2 + (\sigma_{\text{phot}})^2$. Following Whitaker et al. (2010), for each progenitor, the observed SED fluxes were perturbed by a normally distributed, pseudo-random number from a Gaussian distribution with a mean of zero and a standard deviation of the photometric error for each respective filter. From these perturbed flux values, we generated 100 simulated catalogs, and re-determined $U - V$, refitting the photometric redshifts. The uncertainty in $U - V$ color for each progenitor is estimated from the biweight sigma of the its $U - V$ distribution. At each redshift interval, we estimated the values of σ_{phot} for each sample of quiescent and star-forming progenitors by taking the average of the biweight sigma for the progenitors in the considered sample. The average uncertainty in $U - V$ colors for the sample of quiescent progenitors ranges from 0.02 mag at $z = 0.35$ to 0.06 mag at $z = 2.75$, while for the sample of star-forming progenitors it ranges from 0.03 mag at $z = 1.25$ to 0.12 mag at $z = 2.75$.

The derived scatter of the progenitors at $z = 0.35$ is quantitative consistent with the tightness of the red sequence in the local universe ($\sim 0.03 \pm 0.02$ mag; e.g., Bower et al. 1992). While at $0.5 \leq z < 1.0$ the intrinsic scatter in the $U - V$ color is still quite small (~ 0.07 mag), consistent with the scatter of $\sim 0.08 \pm 0.03$ mag from several studies done in galaxy clusters out to $z \sim 0.8$ (van Dokkum 2000; Holden et al. 2004; McIntosh et al. 2005; Mei et al. 2009; Ruhland et al. 2009; van Dokkum 2008), the scatter in the rest-frame $U - V$ color of the quiescent progenitors becomes progressively larger with increasing redshift, i.e., ~ 0.11 mag at $1.0 \leq z < 1.5$ and ~ 0.17 mag at $z > 1.5$. The scatter and its evolution is in good agreement with the evolution of the rest-frame $U - V$ scatter derived from the NEWFIRM Medium-Band Survey (NMBS) in a mass-complete sample of quiescent galaxies at $0.2 < z < 2.2$ with $\log(M_{\text{star}}/M_{\odot}) > 11$ (Whitaker et al. 2010). Our work shows, for the first time, the increasing scatter with redshift of the rest-frame $U - V$ color for a sample of quiescent progenitors of local UMGs rather than for samples selected above a fixed stellar mass at all redshifts and which are likely not evolutionarily connected.

Figure 3 clearly demonstrates that the star-forming progenitors have never lived in the blue star-forming cloud in the last 11.4 Gyr, i.e., since $z = 3$. Indeed, the star-forming progenitors appear to be as red as the quiescent galaxies at all redshifts. In the highest redshift bin, i.e., at $z = 2.75$, quiescent and star-forming progenitors have similar median $U - V$

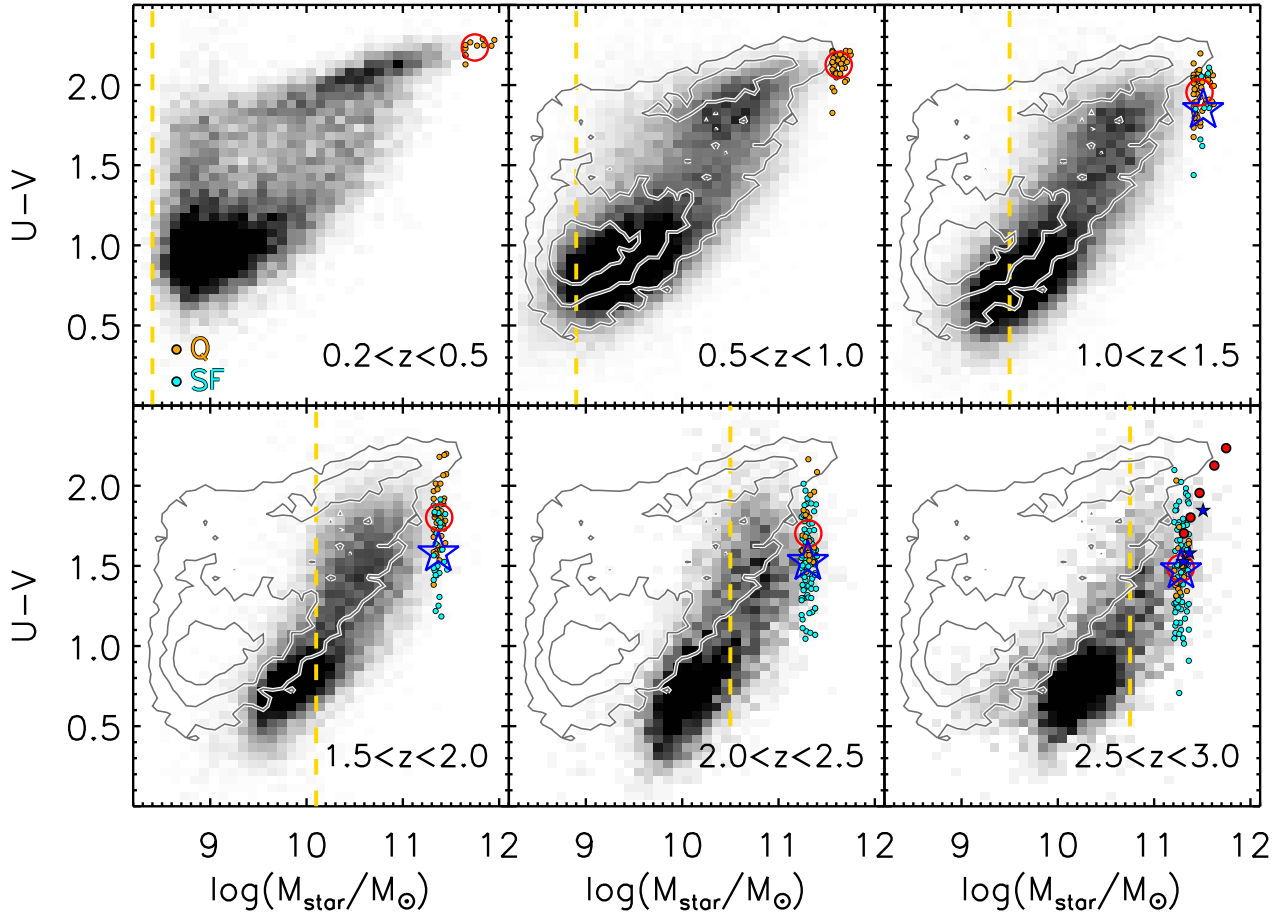


FIG. 3.— Rest-frame $U-V$ color versus stellar mass diagram. The grayscale representation shows the $U-V$ versus M_{star} diagram for the overall galaxy population from the UltraVISTA survey in each redshift interval, with the vertical dashed yellow line representing the 95% completeness in stellar mass. The $U-V$ versus M_{star} diagram at $0.2 \leq z < 0.5$ is overplotted in all panels at $z > 0.5$ as gray contours to highlight the evolution as a function of redshift of the overall galaxy population in the $U-V$ versus M_{star} diagram. Orange and cyan small filled circles represent the quiescent and star-forming progenitors of UMGs. The open red circle and blue star represent the median value of the quiescent and star-forming progenitors, respectively. In the panel corresponding to the $2.5 \leq z < 3.0$ redshift interval, the small filled red circles and blue stars represent the lower redshift median values of the quiescent and star-forming progenitors, respectively, to highlight their evolution with redshift in the color-stellar mass diagram. The star-forming progenitors have never lived in the blue cloud since $z = 3$, and they are as red as the quiescent red-sequence galaxies at all redshifts.

colors, although there is a significant fraction of star-forming progenitors with redder colors compared to most of the quiescent progenitors. The intrinsic scatter in $U-V$ color of the star-forming progenitors is much larger than the quiescent progenitors, i.e., ~ 0.28 mag at $z = 2.75$ and ~ 0.22 mag at $z < 2.5$. As shown in the bottom-right panel of Figure 3, the median $U-V$ color of the star-forming progenitors does not seem to evolve much in the ~ 1.3 Gyr from $z = 2.75$ to $z = 1.75$, whereas the median $U-V$ color of the population of quiescent progenitors becomes redder as it matures from a young, post-starburst to a more evolved population (see also §4.4.1 and 4.5).

The large scatter in $U-V$ of the quiescent progenitors at $z > 1.5$ is evidence that the massive end of the local red sequence is in the process of assembly between $z = 3$ and $z = 1.5$. At $z = 2.75$, $\sim 15\%$ of the progenitors of UMGs have already quenched, most of which only recently (from Fig. 2; see also §4.4.1, 4.4.2, and 4.5). The majority of the progenitors at $z = 2.75$ are star bursting. Then, the quiescent progenitors age with cosmic time and redden, while most of the star-forming progenitors quench in the ~ 2.6 Gyr from $z = 2.75$ to $z = 1.25$. The few remaining star-forming progenitors at $z = 1.25$ com-

plete their migration to the quiescent population before $z = 1$, i.e., in less than 1 Gyr. Therefore, the massive end of the quiescent red sequence is fully formed by $z = 1$, and it ages thereafter in the following ~ 7.7 Gyr from $z = 1$ to $z \sim 0$.

4.4. Evolution in Stellar Population Properties

We now focus on the evolution with redshift of the stellar population properties of the progenitors of UMGs as derived from the modeling of the UV-to- $8\mu\text{m}$ SEDs.

4.4.1. Stellar ages

Figure 4 shows the evolution with redshift of the stellar age derived from SED modeling of the progenitors of UMGs. As stellar age of the galaxy, we adopt the SFR-weighted mean age of the stellar population, $\langle t \rangle_{\text{SFR}}$, as defined in Förster Schreiber et al. (2004). When modeling SEDs, the best-fit age is strictly speaking the time elapsed since the onset of star formation. However, in exponentially declining SFHs, galaxies are continually forming stars, and therefore $\langle t \rangle_{\text{SFR}}$ corresponds more closely to the age of the stars contributing the bulk of the stellar mass (and dominating the light of the galaxy).

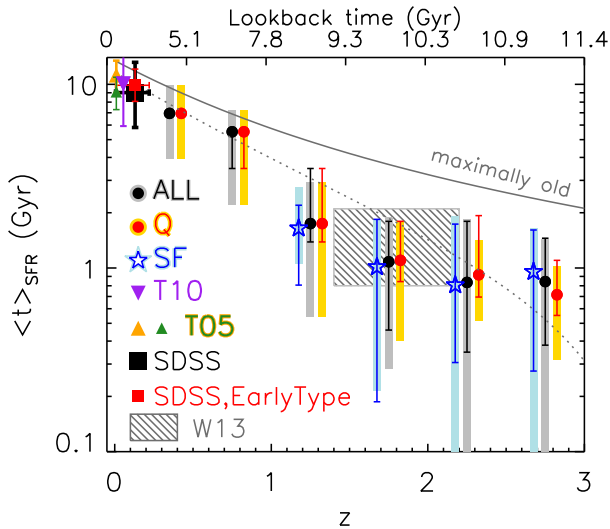


FIG. 4.— Evolution with redshift of the stellar age $\langle t \rangle_{\text{SFR}}$ derived from the modeling of the UV-to- $8\mu\text{m}$ SEDs of the progenitors of local UMGs selected with the semi-empirical approach using abundance matching (black filled circles). Red filled circles and blue empty stars represent the quiescent and star-forming galaxies among the progenitors' sample, respectively. The error bars show the upper and lower ranges including 68% of the populations, while the gray, orange, and light blue filled regions represent the mean 1σ errors in the estimated stellar ages for the whole progenitors' sample, the quiescent, and star-forming progenitors, respectively. The continuous curve represents the age of the universe at the corresponding redshift, while the dotted curve is the continuous curve shifted down by 1.8 Gyr, and going through the measurements at $z \sim 0$. The red and blue symbols are slightly offset along the x-axis (in opposite directions) for clarity. Also plotted are the average age of quiescent galaxies at $1.4 < z < 2.2$ with $\log(M_{\text{star}}/M_{\odot}) > 10.5$ selected from the 3D-HST survey (hatched gray box; Whitaker et al. 2013); the ages of early-type galaxies at $z \sim 0$ with $\log(M_{\text{star}}/M_{\odot}) \approx 11.8$ in high- and low-density environments (orange and green filled upward triangles; Thomas et al. 2005); the age of early-type galaxies at $0.05 < z < 0.06$ with $\log(M_{\text{dyn}}/M_{\odot}) \approx 11.8$ from the SDSS (purple filled downward triangle; Thomas et al. 2010); the typical age of all galaxies at $z \sim 0.13$ with $\log(M_{\text{star}}/M_{\odot}) \approx 11.8$ from the SDSS (black filled square; Gallazzi et al. 2005); and the typical age of early-type galaxies at $z \sim 0.13$ with $\log(M_{\text{star}}/M_{\odot}) \approx 11.8$ from the SDSS (filled red square; Gallazzi et al. 2006). Whereas the median age of the star-forming progenitors remains roughly constant from $z = 3$ to $z = 1$ with ages ~ 0.8 -1.6 Gyr (although with large uncertainties), the median stellar age of the quiescent progenitors increases steadily from $\langle t \rangle_{\text{SFR}} \sim 0.7$ Gyr at $z = 2.75$ to $\langle t \rangle_{\text{SFR}} \sim 7$ Gyr at $z = 0.35$, reaching an age of ~ 9 -10 Gyr by $z \sim 0$.

The typical age of the star-forming progenitors is roughly constant at $\langle t \rangle_{\text{SFR}} \approx 0.8$ -1 Gyr from $z = 3$ to $z = 1.5$, although with a large range of ages spanned at each redshift, and it increases to ~ 1.6 Gyr by $z = 1.25$. The 68% of the population of star-forming progenitors at $z > 1.5$ is bracketed by a lower limit in age of ~ 0.2 -0.3 Gyr and an upper limit in age of ~ 1.6 -1.8 Gyr. On the contrary, the stellar age of the quiescent progenitors increases steadily from $z = 2.75$ (with a median age of ~ 0.7 Gyr) to $z = 0.35$ (with a median age of ~ 7 Gyr). The quiescent progenitors also show a smaller spread in stellar age at each redshift compared to the star-forming progenitors. Specifically, at $z > 1$, the 68% of the quiescent population is bracketed by a lower limit in age $\sim 20\%$ smaller than the median value (compared to 60%-80% for the star-forming progenitors). We note that the stellar ages derived for the star-forming progenitors at $z > 2$ are significantly more uncertain compared to the estimated ages of the quiescent progenitors. As indicated by the orange and light blue filled regions in Figure 4, the formal error on the stellar ages of the star-forming progenitors is 0.7-1.1 Gyr at $z > 2$, a factor of ~ 2 -2.5 larger than for quiescent progenitors at the same redshifts.

Figure 4 clearly shows the aging of the quiescent progenitors of local UMGs with decreasing redshift. This result is also evident from the UVJ diagram shown in Figure 2. Specifically, at $2.5 < z < 3.0$, the quiescent progenitors mostly populate the lower-left corner of the quiescent box. From the comparison with the τ_{100} color evolution track (dark gray curve in Fig. 2), this region in the quiescent box of the UVJ diagram corresponds to ages of 0.8-1.2 Gyr, and even younger ages for non-negligible amounts of dust extinction (see §4.4.3), in good agreement with the ages derived from SED modeling. With decreasing redshift, we see from Figure 2 that the population of quiescent progenitors of UMGs progressively migrates toward the upper-right corner of the quiescent box, clearly showing the aging of the stellar population of the quiescent progenitors as a function of cosmic time.

Whereas the above results are photometrically derived, they agree well with recent results showing the spread in spectroscopically-derived ages of quiescent galaxies at $1.4 < z < 2.2$ from the 3D-HST dataset (Whitaker et al. 2013). Specifically, in Whitaker et al. (2013), massive ($\log(M_{\text{star}}/M_{\odot}) > 10.5$), quiescent galaxies at $1.4 < z < 2.2$ were selected using the UVJ diagram and the 3D-HST grism spectra were used to unambiguously identify metal absorption lines in the stacked spectra, including the G band ($\lambda 4304\text{\AA}$), MgI ($\lambda 5175\text{\AA}$), and NaI ($\lambda 5894\text{\AA}$), and to spectroscopically derive an average age of $1.3^{+0.1}_{-0.3}$ Gyr, in good agreement with our photometrically-derived ages in the overlapping redshift interval (see hatched gray box in Figure 4). Whitaker et al. (2013) also showed that the reddest 80% of the quiescent sample is dominated by metal lines and have older mean stellar ages ($1.6^{+0.5}_{-0.4}$ Gyr), whereas the bluest galaxies have strong Balmer lines and a spectroscopic age of $0.9^{+0.2}_{-0.1}$ Gyr. This range in stellar ages for the population of massive quiescent galaxies at $1.4 < z < 2.2$ is in good agreement with the spread in ages we derived photometrically for the sample of quiescent progenitors of UMGs.

Figure 4 also shows the spectroscopically measured light-weighted ages of $z \sim 0$ UMGs. Specifically, the local measurements plotted in Figure 4 correspond to the typical ages of early-type galaxies at $z \sim 0$ with $\log(M_{\text{star}}/M_{\odot}) \approx 11.8$ in high- and low-density environments (Thomas et al. 2005); the age of early-type galaxies at $0.05 < z < 0.06$ with $\log(M_{\text{star}}/M_{\odot}) \approx 11.8$ from the Sloan Digital Sky Survey (SDSS; Thomas et al. 2010); the typical age of all galaxies at $z \sim 0.13$ with $\log(M_{\text{star}}/M_{\odot}) \approx 11.8$ from the SDSS (Gallazzi et al. 2005); and the typical age of early-type galaxies at $z \sim 0.13$ with $\log(M_{\text{star}}/M_{\odot}) \approx 11.8$ from the SDSS (Gallazzi et al. 2006).

Our study provides the first direct proof in the early universe of the results and implications of the archeological studies of UMGs in the local universe. Specifically, from the study of the local stellar population scaling relations presented in Gallazzi et al. (2006), $z \sim 0$ UMGs appear to have a typical light-weighted ages of ~ 10 Gyr, implying a median formation redshift of $z \approx 1.9$. The inferred scatter in age at the very high-mass end (~ 0.078 -0.088 dex, or ≈ 1.8 -2 Gyr; Gallazzi et al. 2006) implies a formation redshift for UMGs as low as $z \sim 1.1$, and as high as $z \sim 3.9$ -4.2. The formation redshift and spread in age of local UMGs agree remarkably well with our findings and our estimated ages for the progenitors of UMGs. Indeed, at $2 < z < 3$, most of the progenitors of $z \sim 0$ UMGs are star-forming and the massive end of the local quiescent red

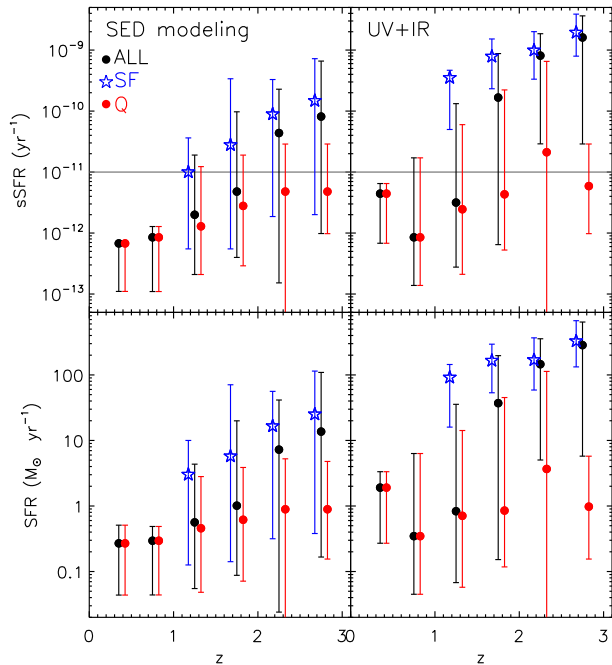


FIG. 5.— Evolution with redshift of the sSFR (top panels) and the SFR (bottom panels) derived from SED modeling (left panels) and from the combination of the UV and IR luminosities (right panels) for the progenitors of UMGs selected with the semi-empirical approach using abundance matching. Symbols as in Fig. 4. The continuous line in the top panels represents the value of $sSFR = 10^{-11} \text{ yr}^{-1}$ typically used in the literature to separate star-forming from quiescent galaxies.

sequence is being vigorously assembled, in agreement with a median formation redshift of UMGs of $z \sim 2$ from archeology studies. As quiescent progenitors are already present at $z = 2.75$, their formation must have started at $z > 3$ for at least some of them, in good agreement with archeological studies in the local universe. This is also quantitatively consistent with recent results showing the existence of very massive galaxies at $3 < z < 4$, and the dominance of star-bursting galaxies at the massive end (Marchesini et al. 2010; Muzzin et al. 2013b). By $1.0 < z < 1.5$, most star-forming progenitors have quenched, in remarkably good agreement with the low formation redshift of $z \sim 1.1$ from the archeological studies of local UMGs. Moreover, assuming that the progenitors of local UMGs start quenching at $2.5 < z < 3.0$ and that their quenching is completed at $1.0 < z < 1.5$ (since no star-forming progenitors are seen at $z < 1$), and assuming passive evolution since $z = 1$, then the mean age difference between the quiescent progenitors of local UMGs should be ~ 2.6 Gyr, i.e., the age difference of the universe between $z = 2.75$ and $z = 1.25$. This is in good agreement with the age dispersion of local UMGs as derived from their fossil records (Gallazzi et al. 2005; Thomas et al. 2005; Gallazzi et al. 2006; Thomas et al. 2010).

4.4.2. Star-formation activity

In this section we present a more quantitative analysis of the evolution with redshift of the SFRs and the specific star-formation rates ($sSFR = SFR/M_{\text{star}}$) of the progenitors of UMGs.

Figure 5 shows the evolution with redshift of the SFRs and sSFR derived from SED modeling (left-hand panels) and from the combination of the UV and IR luminosities (right-

hand panels) for the progenitors of UMGs. At $z \lesssim 1.5$, the progenitors of UMGs are predominantly quiescent, with $sSFR < 10^{-11} \text{ yr}^{-1}$, whereas at $z \gtrsim 1.5$ they become increasingly dominated by star-forming galaxies. The median SFRs of the star-forming progenitors from the combination of the UV and IR luminosities are $\sim 170\text{-}330 M_{\odot} \text{ yr}^{-1}$ at $1.5 < z < 3$, i.e., the star-forming progenitors are intensely star-bursting galaxies, with $sSFR \approx 0.8\text{-}2 \text{ Gyr}^{-1}$, hence doubling their stellar mass in $\sim 0.5\text{-}1.2$ Gyr if these SFRs were to be sustained over this period of time. The evolutions with redshift of the sSFR and SFR derived from SED modeling are qualitatively similar to the evolutions derived from the combination of the UV and IR luminosities, although they differ quantitatively. Specifically, SFRs from the combination of the UV and IR luminosities are typically larger than the SFRs from SED modeling, resulting in larger sSFRs. This is especially true for the star-forming progenitors, most of which are robustly detected in the MIPS $24\mu\text{m}$, with SFRs from the combination of the UV and IR luminosities an order of magnitude larger than the SFRs from SED modeling.

It is worth noting that the progenitors selected as quiescent using the *UVJ* diagram become increasingly more actively star forming at high redshift. The reason for this is twofold. On one hand, the quiescent galaxies at $z > 2$ may indeed have non-negligible levels of star-formation activity. As the early universe is investigated, the quiescent population will be preferentially dominated by post-starburst, relatively younger galaxies whose star-formation activity is still being quenched or has only recently been quenched. On the other hand, contamination of the *UVJ* quiescent population due to misclassified dusty star-bursting galaxies may increase with redshift and be significant at $z > 2$. From the *UVJ* diagram, there is a non-negligible fraction of galaxies at $z > 2$ straddling the quiescent and star-forming regions. Interestingly, most of these galaxies have MIPS $24\mu\text{m}$ detections at $> 5\sigma$, indicative of dusty star-bursting galaxies. The SFRs of $\sim 98\%$ of the quiescent progenitors with robust MIPS detections overlap with the low-SFR tail of the distribution of SFRs of the star-forming progenitors with robust MIPS detections, suggesting that most of the quiescent progenitors with $24\mu\text{m}$ detection may be either transitioning objects from the star-bursting to the quiescent population, or objects in a phase of rejuvenated star formation characterized by relatively low levels of star-formation activity.

It should also be kept in mind that the observed MIPS flux could be potentially contaminated by MIR emission related to obscured AGNs, whose fraction has been shown to increase with stellar mass, especially at higher redshifts (e.g., Kriek et al. 2007). While the relative contributions of star formation and AGN to the $24\mu\text{m}$ flux are difficult to assess here, AGN contamination can be partly responsible for the discrepancy between the SFRs derived from SED modeling and UV+IR, and it may contribute in making some of the *UVJ* quiescent progenitors appear star-forming in Figure 5. We finally note that low MIPS fluxes can also be fully accounted by processes unrelated to obscured AGNs and on-going star formation, such as cirrus dust heated by old stellar populations and circumstellar dust embedding asymptotic giant branch stars (Fumagalli et al. 2013).

We therefore caution against taking the values of the SFRs and sSFRs of the quiescent galaxies at $z > 1.5$ at face value, and argue that these should be interpreted as upper limits due to the potential contamination from dusty star-bursting galaxies and/or obscured AGNs. Even with these caveats, the

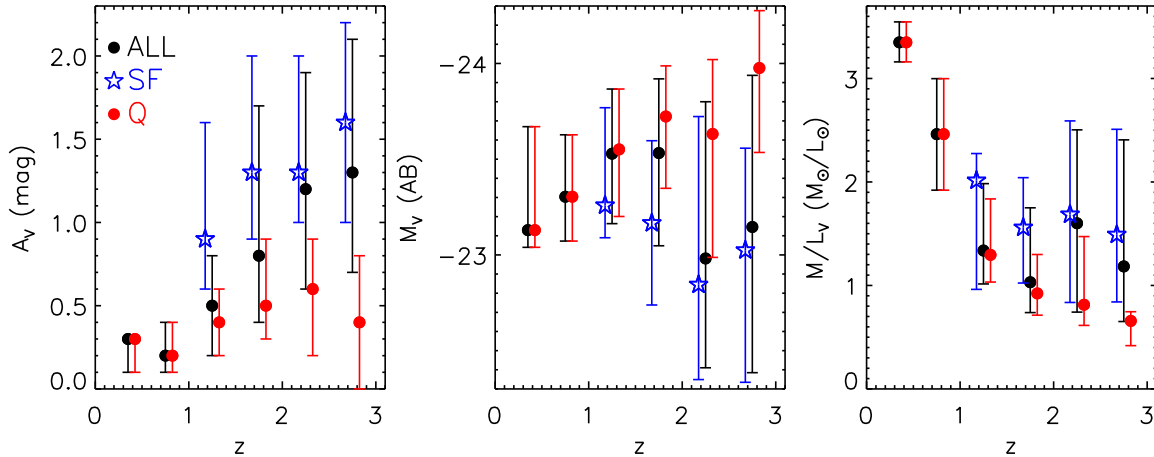


FIG. 6.— Evolution with redshift of the dust extinction (left), the rest-frame V -band absolute magnitude (middle), and the mass-to-light ratio in the rest-frame V -band, M_{star}/L_V , (right) for the progenitors of UMGs selected with the semi-empirical approach using abundance matching. Symbols as in Fig. 4. Dust extinction of the progenitors increases with redshift, driven by the growing importance of dusty star-bursting galaxies among the progenitors at $z > 1.5$. A mild increase of the dust extinction with redshift in the quiescent progenitors is also detected. The M_{star}/L_V of the star-forming progenitors remains roughly constant with redshift, but larger than the M_{star}/L_V of the quiescent progenitors at $z > 1.5$ due to larger dust obscuration. The M_{star}/L_V of the quiescent progenitors increases steadily with cosmic time due to aging of the overall stellar population.

result that the progenitors of UMGs are increasingly dominated by dusty star-bursting galaxies at higher redshifts (i.e., $z > 1.5-2$) is robust.

4.4.3. Dust extinction

The left panel of Figure 6 shows the evolution with redshift of the dust extinction (A_V) derived from the modeling of the UV-to- $8\mu\text{m}$ SEDs. The progenitors of UMGs are progressively dustier with increasing redshift, with the median dust extinction increasing from $A_V \sim 0.3$ mag at $z = 0.35$ to $A_V \sim 1.3$ mag at $z = 2.75$. The observed growth is driven by the growing importance with redshift of the population of dusty starburst galaxies, having a median extinction of $A_V \sim 1.6$ mag and a 68% range of $A_V \sim 1-2.2$ mag at $z = 2.75$. On the contrary the quiescent population is characterized by dust extinction $A_V < 1$ mag over the full targeted redshift interval $0.2 < z < 3.0$.

We note that the quiescent progenitors also show a mild increase with redshift of the dust extinction. Evidence for an increase with redshift of the dust extinction in both the overall and quiescent populations of massive galaxies were previously presented by Whitaker et al. (2010) and Marchesini et al. (2010). Whitaker et al. (2010) found a median extinction of $A_V = 0.2-0.3$ mag in massive ($M_{\text{star}} > 10^{11} M_\odot$) quiescent galaxies at $z \sim 1-2$, in qualitative agreement with the range of A_V found in our sample of quiescent progenitors in the overlapping redshift range. Marchesini et al. (2010) studied a complete sample of galaxies at $3 < z < 4$ with $M_{\text{star}} > 4 \times 10^{11} M_\odot$, finding a median dust extinction of $A_V = 1.4$ mag, in good agreement with the median extinction in our sample of progenitors at $2.5 < z < 3.0$, and evidence of increasing amount of dust in the population of very massive galaxies in the early universe.

4.4.4. Rest-frame absolute V-band magnitude

The central panel of Figure 6 shows the evolution with redshift of the rest-frame V -band absolute magnitude (M_V) derived by integrating the redshifted rest-frame filter bandpass from the best-fit EAZY template, as described in Brammer et al. (2011). This method produces similar rest-

frame luminosities as other methods interpolating between the observed bands that bracket the rest-frame band at a given redshift (e.g., Rudnick et al. 2003).

The progenitors of UMGs have median rest-frame V -band absolute magnitude in the range from $M_V = -23.0$ to $M_V = -23.5$. When the progenitors are separated in quiescent and star-forming galaxies, a clear trend with redshift becomes evident. The star-forming progenitors span a large range in M_V at each redshift (0.7-1.4 mag, depending on the redshift interval). The median rest-frame V -band absolute magnitude of the star-forming progenitors increases with cosmic time from $M_V = -22.9$ at $2 < z < 3$ to $M_V = -23.3$ at $1.0 < z < 1.5$, which correspond to $1.3 \times L_V^*$ and $2.5 \times L_V^*$, respectively (with L_V^* the characteristic luminosity of the rest-frame V -band luminosity function of galaxies at the corresponding redshift; Marchesini et al. 2012). On the contrary, the rest-frame V -band luminosity of the quiescent progenitors decreases with cosmic time from $M_V = -24.0$ (corresponding to $\sim 3.3 \times L_V^*$) at $2.5 < z < 3.0$ to $M_V = -23.1$ (corresponding to $\sim 4 \times L_V^*$) at $0.2 < z < 0.5$.

4.4.5. Mass-to-light ratio

The right panel of Figure 6 shows the evolution with redshift of the mass-to-light ratio M_{star}/L_V . The M_{star}/L_V of the progenitors of UMGs is roughly constant at $z > 1$ ($M_{\text{star}}/L_V \sim 1.1 M_\odot L_\odot^{-1}$) and increases with cosmic time to $M_{\text{star}}/L_V \sim 3.3 M_\odot L_\odot^{-1}$ at $z = 0.35$. The star-forming and quiescent progenitors show once again different dependency of their mass-to-light ratios as a function of redshift. The star-forming progenitors are characterized by a constant mass-to-light ratio, $M_{\text{star}}/L_V \sim 1.7 M_\odot L_\odot^{-1}$, over the entire $1 < z < 3$ redshift range. On the contrary, the mass-to-light ratio of the quiescent progenitors increases steadily with cosmic time, from $M_{\text{star}}/L_V \sim 0.7 M_\odot L_\odot^{-1}$ at $z = 2.75$ to $M_{\text{star}}/L_V \sim 3.3 M_\odot L_\odot^{-1}$ at $z = 0.35$. Interestingly, at $z > 1$, the mass-to-light ratio of the star-forming progenitors is larger than the mass-to-light ratio of the quiescent progenitors by a factor of $\sim 1.5-2.3$ due to the significantly larger amount of dust extinction in the star-forming population. At $z < 1$, the mass-to-light ratio of the quiescent progenitors increases due to the aging (and the

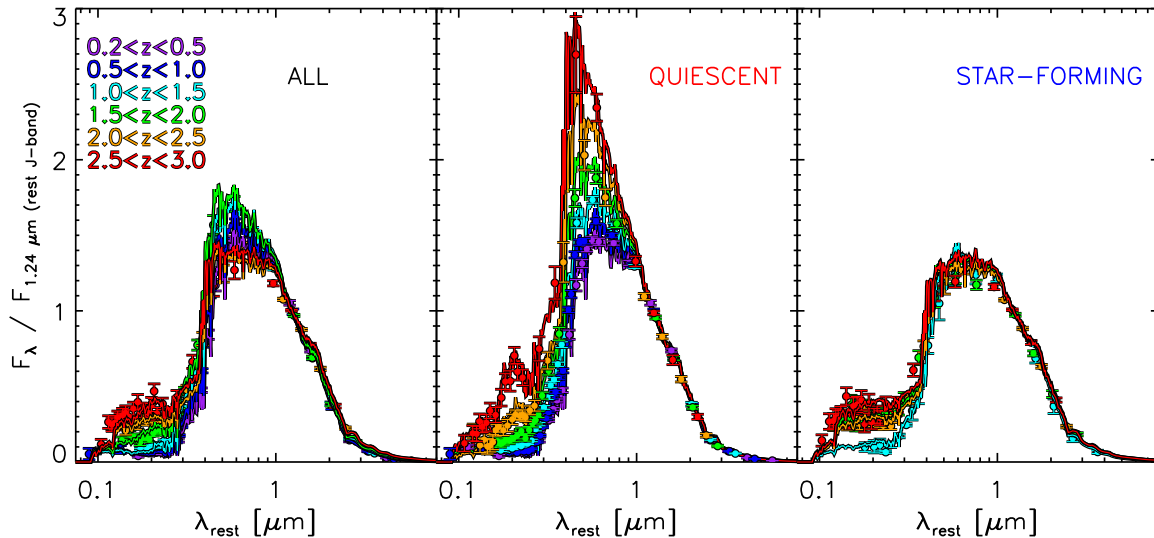


FIG. 7.— Evolution with redshift of the median rest-frame SEDs of the progenitors of UMGs selected with the semi-empirical approach using abundance matching. The left panel shows all progenitors at different redshifts; the middle and right panels show the evolution of the rest-frame SEDs of the quiescent and star-forming progenitors, respectively. Filled colored circles represent the median rest-frame SEDs derived from the observed photometry, whereas the colored curves represent the median best-fits from SED modeling. The SEDs derived from these two methods are in good agreement. The progenitors of UMGs have rest-frame SEDs typical of dusty star-bursting galaxies at high redshift (i.e., $z \gtrsim 2$), whereas their rest-frame SEDs are dominated at low redshifts by the SEDs typical of quiescent galaxies with little or no dust extinction, and old ages. The quiescent progenitors at high redshift have rest-frame SEDs typical of post-starburst galaxies, characterized by strong Balmer breaks and “peaky” rest-frame optical SEDs.

fainting) of the overall stellar population.

4.5. Evolution of the SEDs

Figure 7 shows the evolution of the rest-frame SEDs of the progenitors of UMGs from $z = 3$ to $z = 0.2$, along with the evolution of the rest-frame SEDs of the quiescent and star-forming progenitors (middle and right panels, respectively). The SEDs have been normalized using the flux in the rest-frame J -band (i.e., $\lambda_{\text{rest}} = 1.24 \mu\text{m}$). This figure summarizes the results for the evolution of the stellar population properties found in previous §4.4. Whereas little evolution is seen in the star-forming progenitors (which dominate at $z > 2$), consistently with the derived evolution of their stellar population properties, significant evolution is observed for the quiescent progenitors, which dominate the overall progenitors’ population at $z < 2$. Specifically, the SEDs of the quiescent progenitors evolve from an SED typical of a young post-starburst galaxy with moderate dust extinction at $z = 2.75$ into an SED typical of a quiescent, maximally old stellar population with little or no dust extinction at $z = 0.35$. As Figure 7 shows, the population of progenitors of UMGs was dominated by dusty star-bursting galaxies in the early universe. Such population has mostly quenched by $z \sim 1.5$, with all progenitors having become quiescent by $z = 1$, and has aged thereafter with cosmic time, evolving into a homogeneous population of quiescent, maximally old progenitors by $z = 0.35$.

4.6. Possible systematic effects

In this section we address three possible systematic effects which can potentially bias the results presented in the previous sections, namely systematic errors in photometric redshift estimates, contamination from emission lines, and systematic uncertainties in the modeling of the observed SEDs.

4.6.1. Systematic errors in photometric redshifts

Previous searches for old and massive galaxies at $z > 4$ highlighted the difficulty in unambiguously identifying old

and massive objects at extreme redshifts on the basis of spectral fitting, with equally acceptable solutions between high-redshift very massive galaxies with low-extinction and massive ($10^{11} M_{\odot}$) galaxies with high extinction ($A_V \sim 4$ mag) at intermediate redshifts ($z \sim 2$) (e.g., Dunlop et al. 2007). Moreover, using NIR medium band data from the NMBS, Marchesini et al. (2010) found that the inclusion of an “old and dusty” template in the photometric redshift estimate caused approximately half of the massive galaxies population at $z > 3$ to be consistent with a somewhat lower photometric redshift in the range $2 < z < 3$. Whereas, at present, there is no strong evidence from spectroscopic studies of the existence of such an old and dusty population, Muzzin et al. (2013b) showed that the inclusion of such “old and dusty” template has significant effects on the high-mass end of the stellar mass function of star-forming galaxies at $z > 1.5$, especially at $3 < z < 4$.

Given that at $z > 2$ our sample of progenitors of UMGs are dominated by a population of massive galaxies with very red $U-V$ and $V-J$ colors and significant amount of dust extinction (see Fig. 8 for four representative examples of SEDs), it is worth examining the potential systematic effect of including this “old and dusty” template on the inferred evolution of the progenitors of local UMGs. We have repeated the entire analysis after inclusion of the same “old and dusty” template adopted in Muzzin et al. (2013b). Specifically, we used the corresponding stellar mass functions from Muzzin et al. (2013b) to select progenitors and we studied the evolution of their properties.

Consistently with what found by Marchesini et al. (2010) and Muzzin et al. (2013b), we find that quiescent galaxies are not affected by the inclusion of this new template, whereas the star-forming galaxies with extreme colors tend to systematically shift to lower redshifts. Whereas individual star-forming galaxies at $z > 2$ may change their redshifts substantially, the results agree well qualitatively and quantitatively at $z < 2.5$, with relevant differences only in the highest targeted redshift

bin. Specifically, the progenitors at $2.5 < z < 3.0$ tend to be slightly less massive (by ~ 0.15 dex), less dust extinguished (~ 0.3 mag), and with a slightly bluer median $U - V$ color (by ~ 0.2 mag, although with the same spanned range in $U - V$ color) when the “old and dusty” template is included. Worth noting is also a significant increase in the spanned ranges of rest-frame $U - V$ and $V - J$ colors toward redder values, especially at $2 < z < 2.5$, when the new template is included.

Despite these differences, the overall evolutionary picture of the progenitors of local UMGs does not change at all in, e.g., the $U - V$ versus M_{star} diagram, hence our main results and conclusions are robust against the inclusion of the “old and dusty” template, whose relevance has yet to be confirmed and assessed spectroscopically.

4.6.2. Emission line contamination

Contamination of the photometry from emission lines is another source of systematic effects, potentially resulting in significant overestimated stellar masses. Several recent spectroscopic investigations have shown serious systematic effects due to emission lines on the derived stellar masses of rest-frame UV selected, star-forming galaxies at $z > 4$ (e.g., Bowler et al. 2012; Ellis et al. 2013; Labbé et al. 2013; Stark et al. 2013).

We have used the best-fit EAZY template to quantify the impact of emission lines on the estimated stellar masses. Specifically, the EAZY templates used to derive photometric redshifts include emission lines, and we have measured emission lines equivalent widths on the best-fit EAZY templates of the progenitors’ sample. Then, we used the measured equivalent widths to correct the observed SEDs, and we re-estimated stellar masses using the emission lines corrected SEDs. This modeling leads to conclude that the majority of the progenitors’ sample at $0.2 < z < 3.0$ is not affected significantly by emission line contamination, with a mean difference of 0.03 ± 0.05 dex in the stellar mass estimated before and after emission line correction. We estimate that $\sim 5\%$ of the sample appears to be affected significantly by emission line contamination, with stellar masses overestimated on average by a factor of ~ 2.5 . Since these galaxies represent less than 10% of the sample of star-forming progenitors at $z > 1.5$, we conclude that, based on the emission line ratios and simplistic modeling adopted in EAZY, our results appears to be relatively robust against emission line contamination.

However, we caution that unusually high line ratios, especially $[\text{OIII}]/\text{H}\beta$, are being consistently found in star-forming galaxies at $z > 3$, significantly biasing estimated stellar masses (Holden et al. 2014). While these studies have been currently targeting only rest-frame UV selected galaxies with smaller stellar masses ($\log(M_{\text{star}}/M_{\odot}) < 10.7$) compared to our progenitors’ sample, we stress that a robust quantitative assessment of emission line contamination in the $z > 2$ galaxy population at the high-mass end will necessarily require spectroscopic studies for large samples of massive star-forming galaxies, currently missing.

4.6.3. SED modeling

The derived stellar population properties depend on the adopted choice of SED-modeling assumptions. We have investigated the effects of different SED-modeling assumptions by adopting different SFHs, extinction curves, and metallicities. Specifically, in place of the exponentially-declining SFH we have used a delayed- τ SFH of the form $SFR \propto$

$t \exp(-t/\tau)$, which allows for increasing SFR at earlier times. In place of the Calzetti et al. (2000) extinction curve, we have adopted both the Milky Way extinction law (Cardelli et al. 1989) and the extinction curve proposed by Kriek & Conroy (2013), which assumes a dust attenuation curve with $R_V = 4.05$ and a UV dust bump which is 20% of the strength of the Milky Way bump, following the prescription by Noll et al. (2009). Finally, we have relaxed the assumption on metallicity by leaving it as a free parameter in the SED modeling.

The systematic effects on the stellar population properties of the progenitor galaxies are found to be significantly smaller than the corresponding typical random uncertainties for most of the different SED-modeling assumptions. For the stellar mass, the systematic effect is found to be relevant only when adopting the Milky Way extinction curve, although still comparable to the typical random uncertainty, with M_{star} smaller by 0.05(0.09) dex for the quiescent (star-forming) progenitors. The adoption of the Milky Way extinction curve also results in the largest systematic effects for the dust extinction, although significantly smaller compared to its typical random uncertainty, with A_V smaller by 0.05(0.2) mag for the quiescent (star-forming) progenitors compared to the case when the Calzetti et al. (2000) law is adopted. The largest effect on the star-formation rate for the quiescent progenitors is found when the delayed- τ model is adopted, with SFR smaller by 0.1 dex, whereas the largest effect on the star-formation rate for the star-forming progenitors is found when the Milky Way extinction curve is adopted, with SFR smaller by 0.13 dex. Finally, the largest effects on the stellar ages of the star-forming progenitors are found when the delayed- τ model is adopted, with $\langle t \rangle_{\text{SFR}}$ larger by ~ 0.1 dex compared to the default SED-modeling assumptions. The stellar ages of the quiescent progenitors changes at most by 0.02 dex depending on the different SED-modeling assumptions. We therefore conclude that the inferred evolution with redshift of the stellar population properties of the quiescent and star-forming progenitors of local UMGs are robust and not very sensitive to reasonable choices of the SED-modeling assumptions.

However, systematic effects in the modeling of the observed SEDs, and hence in the estimated stellar masses, can be relevant in galaxies characterized by composite stellar populations. Specifically, the stellar masses of the dusty, massive star-forming progenitors at $z > 1.5$ could be potentially overestimated when modeled with a single stellar population, especially if characterized by multiple stellar population components with differential dust extinctions, such as a quiescent un-obscured population and a young, dusty star-bursting component.

To investigate potential biases in the stellar masses of the star-forming progenitors at $2 < z < 3$, we have derived stellar masses by allowing for multiple stellar components to contribute to the observed SEDs of the dusty star-forming progenitors. No systematic differences are found, with a median difference smaller than 0.1 dex and a scatter of ~ 0.5 dex (Brammer et al. 2014, in preparation). We also note that the observed SEDs of most of the dusty star-forming progenitors of UMGs at $z > 1.5$ cannot be well modeled by an ad hoc combination of a quiescent un-obscured population and a young, dusty star-bursting component, which would arguably cause the largest biases in the stellar mass estimates (Brammer et al. 2014, in preparation).

We therefore conclude that, while the stellar masses of individual star-forming progenitors may be systematically different by a factor of a few-to-several due to simplified SED-

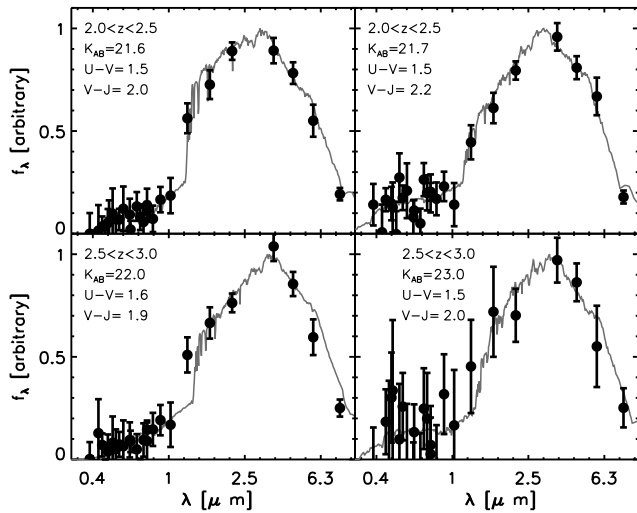


FIG. 8.— Examples of SEDs of reddest star-forming progenitors with $V - J > 1.9$. Black filled circles and error bars represent the observed photometry, whereas the continuous gray curve shows the best-fit model. The top and bottom rows show SEDs at $2.0 < z < 2.5$ and $2.5 < z < 3.0$, respectively.

modeling assumptions, the stellar mass distribution of the overall population appears to be largely unaffected by the adopted SED-modeling assumptions. Nonetheless, we stress that the multi-component modeling in Brammer et al. (2014) is still over simplified (e.g., a dust screen with an adopted Calzetti et al. 2000 extinction curve), and systematic errors up to a factor of several in stellar mass cannot be excluded for a subset of the most extreme star-forming progenitors.

4.6.4. The reddest star-forming progenitors: a new population?

In this study we have demonstrated that a significant fraction of the progenitors of UMGs at $z > 2$ are dusty star-forming galaxies. Amongst that population, $\sim 19\%$ have extraordinary SEDs with very red $V - J$ colors ($V - J > 1.9$). As shown in Figure 2, effectively zero galaxies with such red $V - J$ colors exist at $z < 1$ (down to the UltraVISTA mass limit), and therefore it is tempting to classify them as a “new” population of galaxies.

These extremely red galaxies are intriguing, and in Figure 8 we show four representative examples of their SEDs. The solid lines are the best-fit FAST SEDs using the default SED modeling assumptions. The fits are reasonable and hence with the default assumptions we naturally interpret this population as massive, extremely red, star-forming progenitors. However, the SEDs are quite unlike local galaxies, and given that they only appear at $z > 1$, it is important to consider carefully what else this unusual population might be and how accurate their stellar masses are. As already discussed, systematic effects likely dominate the uncertainties in both the photometric redshifts and SED modeling of individual galaxies among this extreme population.

Specifically, strong emission lines (or unusual emission-line ratios) could result in significantly overestimated stellar masses, while the presence of optically thick regions could even cause the underestimating of their stellar masses. Perhaps of most concern are composite stellar populations and/or potential blending/confusion of sources in ground-based images which could result in the unusual SEDs and therefore biased stellar masses.

Without additional data it is difficult to say how reasonable the SED modeling assumptions are for this population, and how reliable their stellar masses are. Therefore, currently we advise caution in interpreting this extreme population. While they are only $\sim 19\%$ of the overall population, and unlikely to change our overall picture of UMG formation, they are intriguing, and detailed investigations, beyond the capabilities of current photometric catalogs, will be needed to confirm the existence of this population, and to assess its relevance in the formation of massive galaxies in the early universe.

We note that a better understanding of this population could be made with current instrumentation. Spectroscopy from ground-based near-infrared spectrographs and ALMA could measure spectroscopic redshifts and clearly identify the level of contamination of the broad band colors from emission lines (if any). Likewise, *Hubble Space Telescope* near-infrared observations could resolve them spatially and be used to test for confusion/blending, as well as potential systematics from resolved composite stellar populations. Lastly, deep spectroscopy could be used to determine velocity dispersions, which will be the key for understanding how reliable the photometrically-derived masses are. Followup of this extreme population will be key for a more complete understanding of the evolutionary history of UMGs.

5. SUMMARY AND CONCLUSIONS

In this paper we have investigated the evolution since $z = 3$ of the properties of the progenitors of ultra-massive galaxies ($\log(M_{\text{star}}/M_{\odot}) \approx 11.8$) at $z = 0$ (UMGs). The progenitors have been selected using the fixed cumulative number density approach and a semi-empirical method using abundance matching in the Λ CDM paradigm. When the progenitors are selected with the fixed cumulative number density approach, the stellar mass of the progenitors is seen to grow by a factor of ~ 2.2 from $z = 3$ to $z = 0$, implying that about half of the stellar mass in local UMGs was assembled at $z > 3$. If the progenitors are selected with the semi-empirical method using abundance matching, the evolution in stellar mass is much more significant ($0.56^{+0.35}_{-0.25}$ dex), with only about a fourth of the stellar mass in local UMGs having been assembled by $z = 3$. Since the semi-empirical approach using abundance matching accounts for merging, whereas the fixed cumulative number density method does not, the former is a more desirable and robust approach to constrain the evolution of the median cumulative number density and therefore to select progenitors. The comparison between the assembly history of local brightest cluster galaxies (BCGs) as predicted from semi-analytic models with the inferred evolution in stellar mass since $z = 3$ of the progenitors of local UMGs provides yet another manifestation of the previously highlighted tensions between the observed and model-predicted evolutions of the stellar mass function since $z = 4$ (e.g., Marchesini et al. 2009). Specifically, low-mass galaxies in the stellar mass range $10^9 - 10^{11} M_{\odot}$ form too early in the models and are too passive at later times (Fontanot et al. 2009), with the mass growth of simulated BCGs being dominated by accretion since $z \sim 4$ (De Lucia & Blaizot 2007), in contrast to what is measured in our study.

The progenitors of UMGs have been separated in quiescent and star-forming galaxies using the rest-frame $U - V$ versus $V - J$ diagram (UVJ diagram). At $z = 0.35$, the progenitors of UMGs constitute a homogeneous population with similar rest-frame $U - V$ and $V - J$ colors, typical of quiescent galaxies with old stellar populations (age ~ 7 Gyr). As the progenitors

are followed to higher redshifts, this population becomes increasingly diversified. At $z < 1$, the progenitors are all quiescent, while at $z > 1$ the contribution from star-forming galaxies progressively increases, with the progenitors' population being dominated by dusty, star-bursting galaxies at $2 < z < 3$.

The stellar population properties (i.e., stellar age, dust extinction, star-formation rate, specific star-formation rate, rest-frame absolute V -band magnitude, and mass-to-light ratio in the rest-frame V band) have been estimated from the modeling of the UV-to- $8\mu\text{m}$ spectral energy distributions and $24\mu\text{m}$ data, and their evolutions with redshift have been investigated. At $z = 2.75$, most of the progenitors of UMGs are dusty ($A_V \sim 1.2\text{--}2.2$ mag) star-bursting ($\text{SFR} \sim 100\text{--}700 M_\odot \text{ yr}^{-1}$; $\text{sSFR} \sim 0.8\text{--}4 \text{ Gyr}^{-1}$) galaxies with a large range in stellar ages, i.e., $0.3\text{--}1.6$ Gyr. At the same redshift, the quiescent progenitors have properties typical of young (age $\sim 0.6\text{--}1$ Gyr) post-starburst galaxies with little dust extinction ($A_V \sim 0.4$ mag) and strong Balmer breaks, showing a large scatter in rest-frame $U - V$ color (~ 0.2 mag). With decreasing redshift, the fraction of quiescent progenitors increases as the star-forming progenitors quench to build the quiescent population. At the same time, the stellar population of the already quiescent progenitors is clearly seen to age with cosmic time, with their properties changing accordingly. Specifically, their stellar ages and mass-to-light ratio increase with decreasing redshift, and their median SEDs evolve from being characterized by a strong Balmer break to being shaped by the 4000\AA break in the rest-frame optical. Moreover, the quiescent progenitors are seen to migrate from the bottom-left to the upper-right corner of the UVJ quiescent box and their rest-frame $U - V$ color to redden, as expected from an aging quiescent stellar population.

It is interesting to note that the stellar properties of the star-forming progenitors do not appear to be changing substantially over the redshift interval $1.5 < z < 3.0$, and that over this same interval the scatter in the $U - V$ color of the quiescent progenitors remains constant and large (~ 0.17 mag) and it starts to decrease only at $z < 1.5$. It appears indeed that $z = 1.5$ marks the time by which most of the star-forming progenitors have quenched, as indicated by the very few star-forming progenitors at $1.0 < z < 1.5$. Consistent with this interpretation, the last star-forming progenitors to quench at $z = 1.25$ are characterized by lower levels of star formation and older ages on average compared to the star-forming progenitors at $z > 1.5$. By $z = 1$, all star-forming progenitors have quenched, and the quiescent progenitors are simply left aging thereafter in the following ~ 7.7 Gyr to $z = 0$, and some additional growing due to, e.g., minor dry mergers.

Whereas the existence at $z = 2.75$ of a small fraction ($\sim 15\%$) of quiescent progenitors implies that the assembly of the very massive end of the local quiescent red-sequence population must have started at $z > 3$, our results suggest it had been mostly assembled between $z = 3$ and $z = 1.5$, with all the growth by in-situ star formation ceased by $z = 1$. Most of the quenching of the star-forming progenitors is seen to happen between $z = 2.75$ and $z = 1.25$, implying a mean age difference of ~ 2.6 Gyr among the UMGs. Our results are in remarkably good agreement with the typical formation redshift of quiescent, red-sequence UMGs in the local universe ($z \sim 1.9$) and their rms scatter in age ($\approx 1.8\text{--}2$ Gyr) as derived from archeological studies (e.g., Gallazzi et al. 2006), and provide a direct probe in the early universe of the results and implications of the fossil records in the population of UMGs today.

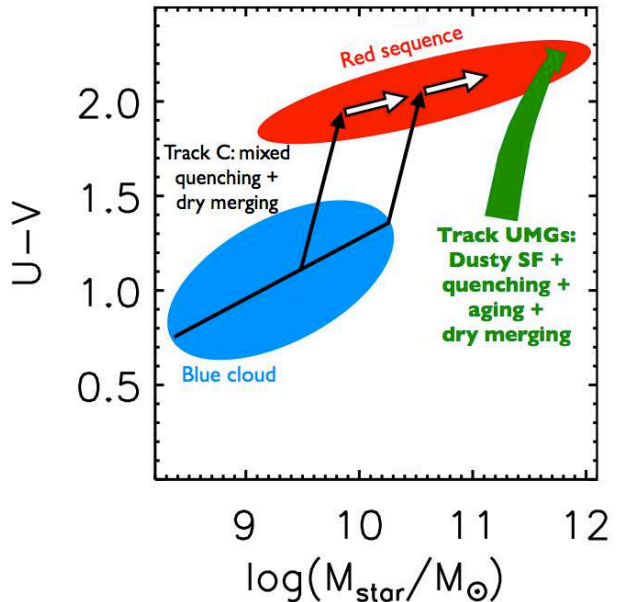


FIG. 9.— Schematic evolutionary tracks plotted in the color-mass diagram showing possible paths for the formation of massive red-sequence galaxies in the local universe. Track C, proposed by Faber et al. (2007), is a “mixed” scenario involving both early and late quenching of blue, star-forming galaxies. The red sequence galaxy arise from the blue galaxy when star formation is quenched (upward black arrows from the blue cloud to the red sequence). Once the galaxy arrives on the red sequence, it may evolve more slowly along it through a series of dry mergers (white arrows). The green arrow represents our newly proposed path for the formation of UMGs in the local universe based on our findings. This new scenario involves in-situ early stellar growth during a short and intense dusty burst of star formation at which point the progenitor manifest as a red, massive, heavily dust-extincted star-bursting galaxy. After quenching, the progenitor continues reddening due to aging and potentially growing in mass via dry mergers, reaching its final position on the color-mass diagram. In this new scenario, the progenitor of local UMGs have never lived on the blue star-forming cloud since $z = 3$. The population of red galaxies is seen to change with cosmic time, dominated by dusty star-bursting galaxies at $z > 2$ and by quiescent galaxies at lower redshift.

Finally, we have shown that the progenitors of UMGs have never lived on the blue star-forming cloud in the last 11.4 Gyr of cosmic history, i.e., since $z = 3$. This is true also for the star-forming progenitors, which have a median rest-frame $U - V$ color at $z = 2.75$ similar to the quiescent progenitors, with a significant fraction of them having $U - V$ colors much redder than most of the quiescent progenitors at the same redshift. In light of our findings, the picture in which early-type UMGs at $z \sim 0$ have formed from star-forming galaxies living on the blue cloud that reddened after quenching and further grew through moderate dry merging has to be refined. Such scenario is pictured in Figure 9 as taken from the “Evolution Track C” in Faber et al. (2007). This scenario involves early mass assembly and star formation in galaxies on the blue cloud of star-forming galaxies. When the star-formation activity in the blue galaxies gets quenched, they rapidly move onto the red sequence. Once on the red sequence of quiescent galaxies, any further growth in stellar mass in these progenitors mostly proceeds via dry merging among galaxies on the red sequence. Whereas such path is still viable to explain the formation of less massive (e.g., $10^{11} M_\odot$) local red-sequence galaxies which may have gone through mostly unobscured (hence blue) episodes of early star formation, our study suggest an alternative path for the formation of UMGs at $z \sim 0$. This new scenario, pictured as a green arrow in Fig-

ure 9, involves early mass assembly and stellar growth in a short and intense dusty burst of star formation during which the progenitors manifest as a red, heavily dust-obscured starbursting galaxies. After quenching, the progenitors continue reddening due to the aging of their stellar populations, and eventually grow in mass through (mostly minor) dry merging, finally reaching their current positions on the color-mass diagram. This scenario qualitatively agrees with the predictions from the theoretical model of the co-evolution of massive galaxies and super-massive black holes originally proposed in Granato et al. (2004) and further developed in Cai et al. (2013) and Lapi et al. (2014), which indicates that the star formation in the progenitors of local very massive spheroids proceeded within a heavily dust-enshrouded medium at $z > 1.5$ over a timescale $\lesssim 0.5 - 1$ Gyr.

Our study provides a complete and consistent picture of how the most massive galaxies in the local universe have formed and assembled since $z = 3$. While we see the star-forming progenitors disappearing and turning into the quiescent progenitors, we do not know what physical mechanisms are responsible for halting the star formation. Is the AGN, if present, playing a major role? What about feedback from the starburst itself? For the first time, our analysis provides a sample of star-forming progenitors that must quench by $z = 1$. Detailed studies of the AGN content, physical conditions of the gas (e.g., gas fraction and gas-phase metallicity), stellar population properties (e.g., stellar ages and metallicities, SFRs), structural and dynamical properties, and environment of these star-forming progenitors can shed light into the physical processes responsible for the inevitable quenching of their star-formation activity. High S/N optical and near-infrared spectroscopic studies, as well as deep sub-millimeter studies with ALMA will provide the datasets to answer the remaining outstanding questions.

Needless to say, our study needs to be extended to earlier times to investigate the properties of the progenitors at $z > 3$, i.e., in the first 2 billion years of cosmic history. Have the progenitors ever lived on the blue star-forming cloud? Which are the progenitors of the quiescent, massive, post-starburst galaxies we see at $2.5 < z < 3$? Much deeper near-infrared selected catalogs over a large surveyed area are required to push this investigation to higher redshift. The second data release (DR2) of the UltraVISTA survey will provide much deeper near-infrared coverage over $\sim 70\%$ of the full COSMOS field, reaching ~ 1.2 mag deeper in the K_S band, and allowing to probe the stellar population 0.5 dex deeper in stellar mass.

The observed assembly since $z = 3$ of the most massive galaxies need to be investigated in more detail in the context of theoretical models of galaxy formation and evolution. The new generation of semi-analytic models accounting for

a better treatment of satellite galaxies, for the formation of the intra-cluster component, including detailed chemical enrichment models, and coupled with radiative transfer codes or templates to predict the infrared luminosities of model galaxies (e.g., Vega et al. 2005; Lagos et al. 2012) will provide valuable tools to further test the physical mechanisms driving the formation and evolution of today’s most massive galaxies.

Finally, we note that $\sim 19\%$ of the star-forming progenitors at $z > 2$ have extraordinary SEDs with very red $V - J$ colors ($V - J > 1.9$), potentially representing a “new” population of galaxies in the early universe that effectively disappear by $z \sim 1$. While unlikely to change our overall picture of the formation of UMGs, systematic effects dominate the uncertainties in both the photometric redshifts and SED modeling of individual galaxies among this extreme population. Detailed investigations, including spectroscopy with near-infrared spectrographs and ALMA, and near-infrared imaging with the *Hubble Space Telescope*, will be needed to confirm the existence of this intriguing population and for a more complete understanding of the evolutionary history of UMGs.

We are grateful to the anonymous referee whose comments and suggestions helped improving significantly this paper. We gratefully acknowledge Peter Behroozi for providing the code implementing the semi-empirical approach using abundance matching to select progenitors. DM acknowledges the support of the Research Corporation for Science Advancement’s Cottrell Scholarship. DM also acknowledges support from Tufts University Mellon Research Fellowship in Arts and Sciences. AM and MF acknowledge support from the Netherlands Foundation for Research (NWO) Spinoza grant. MS acknowledges support from the programs HST-GO-12286.11 and HST-GO-12060.95, provided by NASA through a grant from the Space Telescope Science Institute, which is operated by the Association of Universities for Research in Astronomy, Incorporated, under the NASA contract NAS5-26555. BMJ and JPUF acknowledge support from the ERC-StG grant EGG5-278202. JSD acknowledges the support of the European Research Council through the award of an Advanced Grant, and the support of the Royal Society via a Wolfson Research Merit Award. JSD also acknowledges the contribution of the EC FP7 SPACE project ASTRODEEP (Ref.No: 312725). The Dark Cosmology Centre is funded by the DNRF. This study is based on data products from observations made with ESO Telescopes at the La Silla Paranal Observatory under ESO programme ID 179.A-2005 and on data products produced by TERAPIX and the Cambridge Astronomy Survey Unit on behalf of the UltraVISTA consortium.

APPENDIX

EVOLUTION OF THE PROPERTIES OF PROGENITORS OF UMGs SELECTED USING THE FIXED CUMULATIVE NUMBER DENSITY METHOD

Here we present the evolution of the properties of the progenitors of local UMGs selected using the fixed cumulative number density method. Figures A10 and A11 show the evolution of the UVJ diagram and the $U - V$ versus M_{star} diagram, respectively. Figures A12, A13, and A14 show the evolution as a function of redshift of the stellar age, SFR and sSFR, and dust extinction, rest-frame V -band magnitude, and mass-to-light ratio, respectively. Finally, Figure A15 shows the evolution of the SEDs as a function of redshift. As shown by these figures, the evolution in the stellar population parameters (e.g., rest-frame colors, level of star formation activity, stellar ages, extinction, rest-frame optical absolute magnitudes, and mass-to-light ratios) inferred when the progenitors are selected with the fixed cumulative number density method is qualitatively similar and quantitatively consistent to the evolution obtained when the progenitors are selected adopting the semi-empirical approach using abundance matching.

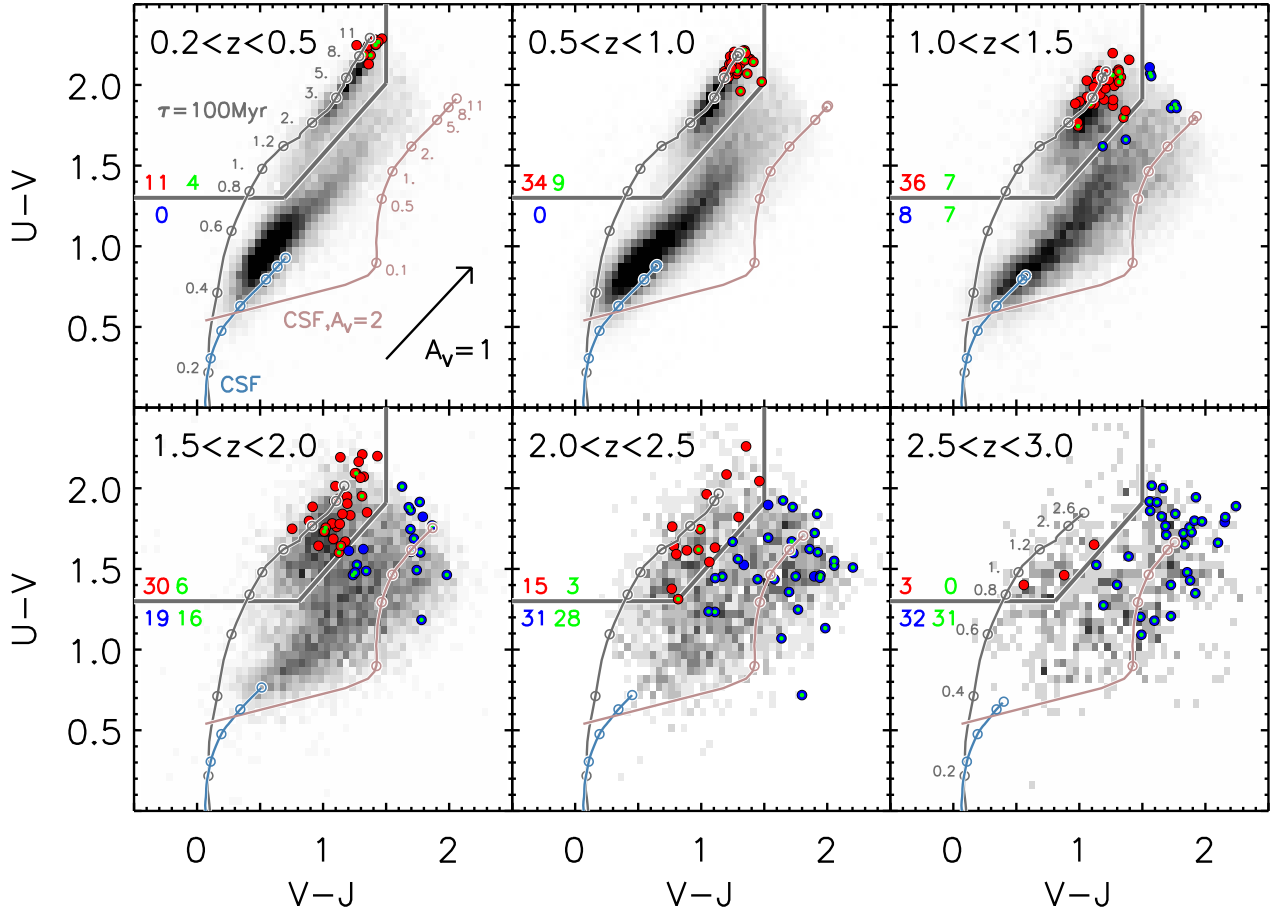


FIG. A10.— Rest-frame $U-V$ versus $V-J$ diagram in the targeted redshift intervals between $z = 0.2$ and $z = 3.0$ for the progenitors of local UMGs selected with the fixed cumulative number density approach. Symbols as in Figure 2.

REFERENCES

- Baldry, I. K., et al. 2006, *MNRAS*, 373, 469
 Baugh, C. M. 2006, *RPP*, 69, 3101
 Behroozi, P. S., Wechsler, R. H., & Conroy, C. 2013a, *ApJ*, 770, 57
 Behroozi, P. S., Marchesini, D., Wechsler, R. H., Muzzin, A., Papovich, C., Stefanon, M. 2013b, *ApJ*, 777, L10
 Bell, E. F., McIntosh, D. H., Katz, N., & Weinberg, M. D. 2003, *ApJS*, 149, 289
 Bell, E. F., et al. 2004, *ApJ*, 608, 752
 Bell, E. F., Papovich, C., Wolf, C., et al. 2005, *ApJ*, 625, 23
 Blanton, M. R., & Moustakas, J. 2009, *ARA&A*, 47, 159
 Bower, R. G., Lucey, J. R., & Ellis, R. S. 1992, *MNRAS*, 254, 601
 Bowler, R. A. A., et al. 2012, *MNRAS*, 426, 2772
 Brammer, G. B., van Dokkum, P. G., & Coppi, P. 2008, *ApJ*, 686, 1503
 Brammer, G. B., et al. 2011, *ApJ*, 739, 24
 Bruzual, G., & Charlot, S. 2003, *MNRAS*, 344, 1000
 Cai, Z.-Y. et al. 2013, *ApJ*, 768, 21
 Calzetti, D., Armus, L., Bohlin, R. C., Kinney, A. L., Koornneef, J., & Storchi-Bergmann, T. 2000, *ApJ*, 533, 682
 Capak, P., et al. 2007, *ApJS*, 172, 99
 Cardelli, J. A., Clayton, G. C., & Mathis, J. S., 1989, *ApJ*, 345, 135
 Cimatti, A., Daddi, E., & Renzini, A. 2006, *A&A*, 453, L29
 Conroy, C., & Wechsler, R. H. 2009, *ApJ*, 696, 620
 Dale, D. A., & Helou, G. 2002, *ApJ*, 576, 159
 De Lucia, G., Springel, V., White, S. D. M., Croton, D., Kauffmann, G. 2006, *MNRAS*, 366, 499
 De Lucia, G., & Blaizot, J. 2007, *MNRAS*, 375, 2
 Draine, B. T., & Li, A. 2007, *ApJ*, 657, 810
 Dunlop, J. S., Cirasuolo, M., & McLure, R. J. 2007, *MNRAS*, 376, 1054
 Elbaz, D., Hwang, H. S., Magnelli, B., et al. 2010, *A&A*, 518, L29
 Ellis, R. S., et al. 2013, *ApJ*, 763, L7
 Faber, S. M., et al. 2007, *ApJ*, 665, 265
 Fontanot, F., De Lucia, G., Monaco, P., Somerville, R. S., Santini, P. 2009, *MNRAS*, 397, 1776
 Förster Schreiber, N. M., et al. 2004, *ApJ*, 616, 40
 Franx, M., van Dokkum, P. G., Förster Schreiber, N. M., Wuyts, S., Labbé, I., & Toft, S. 2008, *ApJ*, 688, 770
 Fumagalli, M., et al. 2013, *ApJ* submitted [arXiv:1308.4132]
 Gallazzi, A., Charlot, S., Brinchmann, J., White, S. D. M., & Tremonti, C. A. 2005, *MNRAS*, 362, 41
 Gallazzi, A., Charlot, S., Brinchmann, J., & White, S. D. M. 2006, *MNRAS*, 370, 1106
 Genzel, R., & Cesarsky, C. J. 2000, *ARA&A*, 38, 761
 Gonzalez-Perez, V., Lacey, C. G., Baugh, C. M., Lagos, C. D. P., Helly, J., Campbell, D. J. R. 2014, *MNRAS*, 439, 264
 Granato, G., De Zotti, G., Sila, L., Bressan, A., Danese, L. 2004, *ApJ*, 600, 580
 Holden, B. P., Stanford, S. A., Eisenhardt, P., & Dickinson, M. 2004, *AJ*, 127, 2484
 Holden, B. P., et al. 2014, *ApJ* submitted [arXiv:1401.5490]
 Henriques, B. M. B., White, S. D. M., Lemson, G., Thomas, P. A., Guo, Q., Marleau, G.-D., Overzier, R. A. 2012, *MNRAS*, 421, 2904
 Ilbert, O., et al. 2013, *A&A*, 556, A55
 Janowiecki, S., Mihos, J. C., Harding, P., Feldmeier, J. J., Rudick, C., Morrison, H. 2010, *ApJ*, 715, 972
 Kauffmann, G., et al. 2003a, *MNRAS*, 341, 54
 Kauffmann, G., et al. 2003b, *MNRAS*, 346, 1055
 Kauffmann, G., et al. 2004, *MNRAS*, 353, 713
 Kennicutt, R. C. 1998, *ApJ*, 498, 541

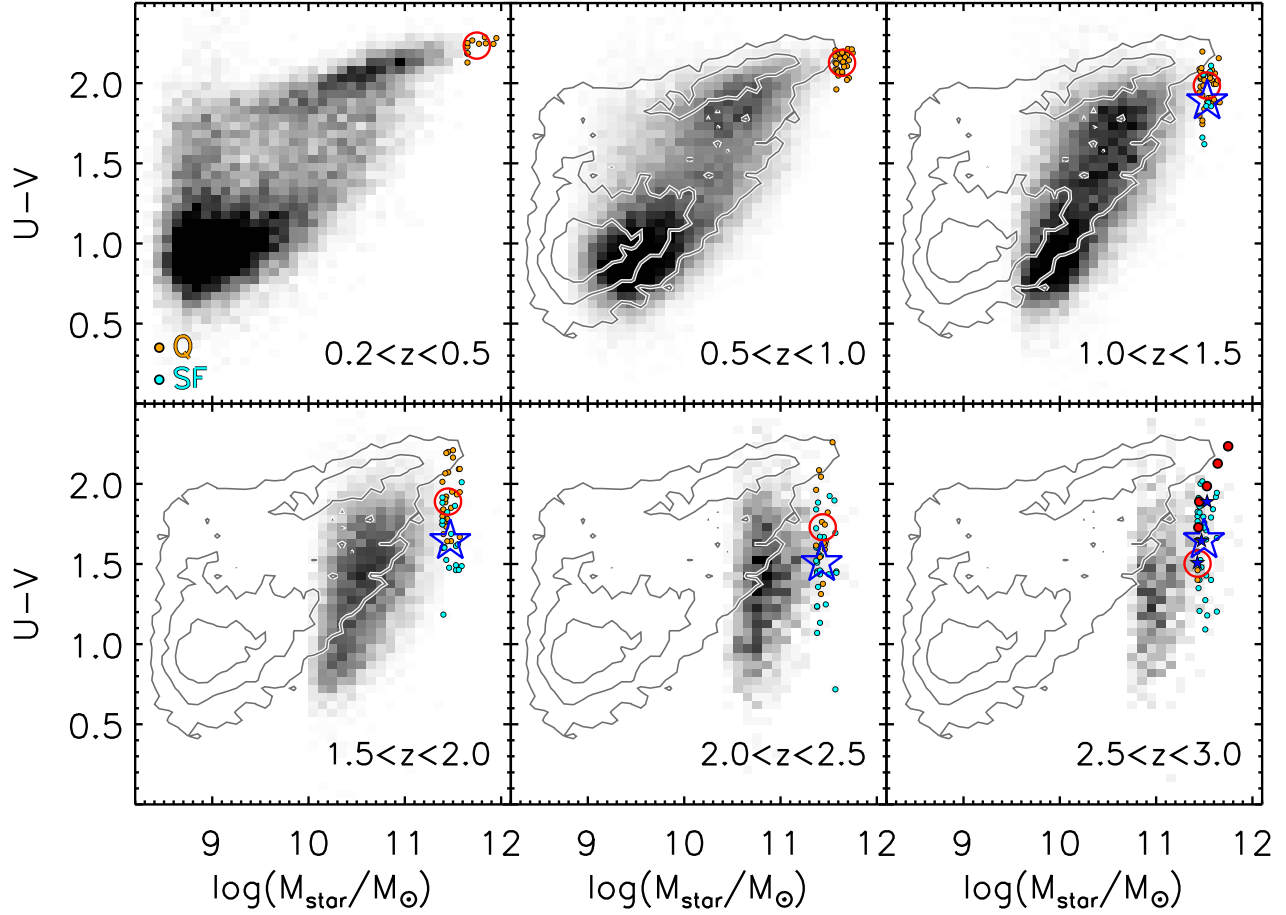


FIG. A11.— Rest-frame $U-V$ color versus stellar mass diagram for the progenitors of local UMGs selected with the fixed cumulative number density approach. Symbols as in Figure 3.

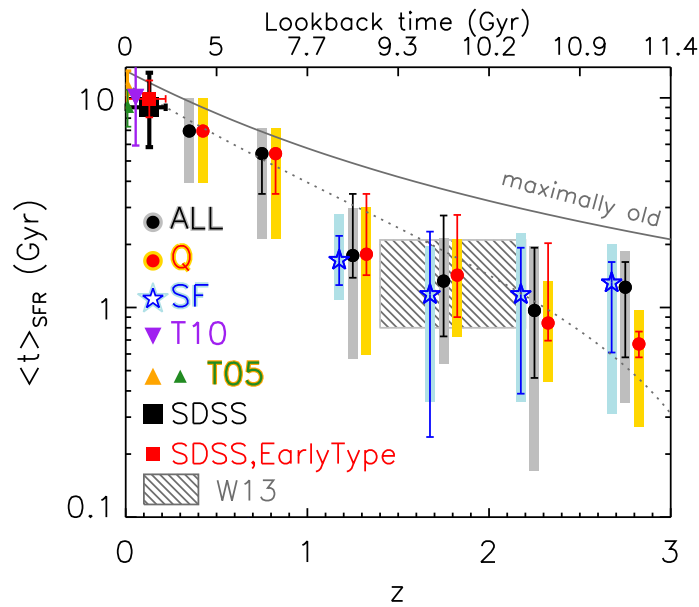


FIG. A12.— Evolution with redshift of the stellar age $\langle t \rangle_{\text{SFR}}$ derived from the modeling of the UV-to- $8\mu\text{m}$ SEDs of the progenitors of local UMGs selected with the fixed cumulative number density approach. Symbols as in Figure 4.

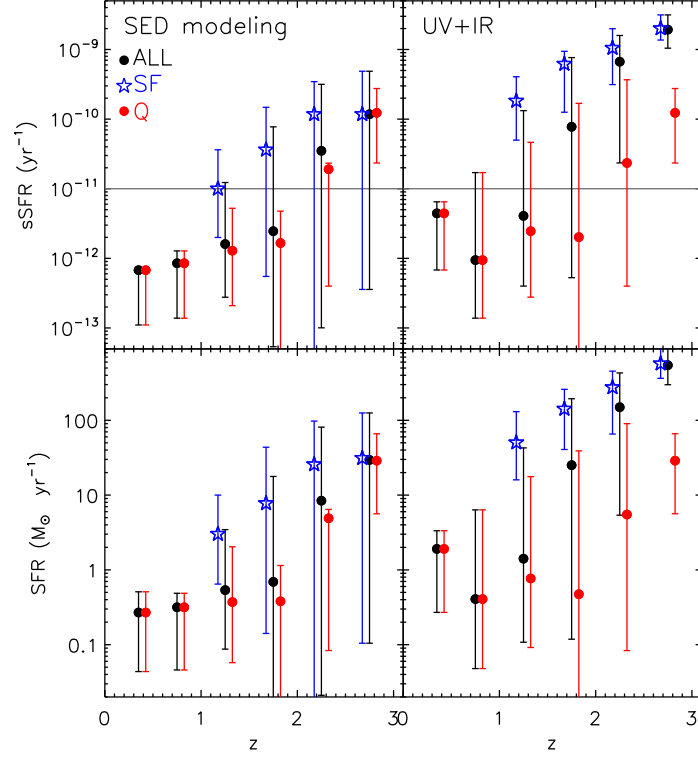


FIG. A13.— Evolution with redshift of the sSFR (top panels) and the SFR (bottom panels) derived from SED modeling (left panels) and from the combination of the UV and IR luminosities (right panels) for the progenitors of UMGs selected with the fixed cumulative number density approach. Symbols as in Figure 5.

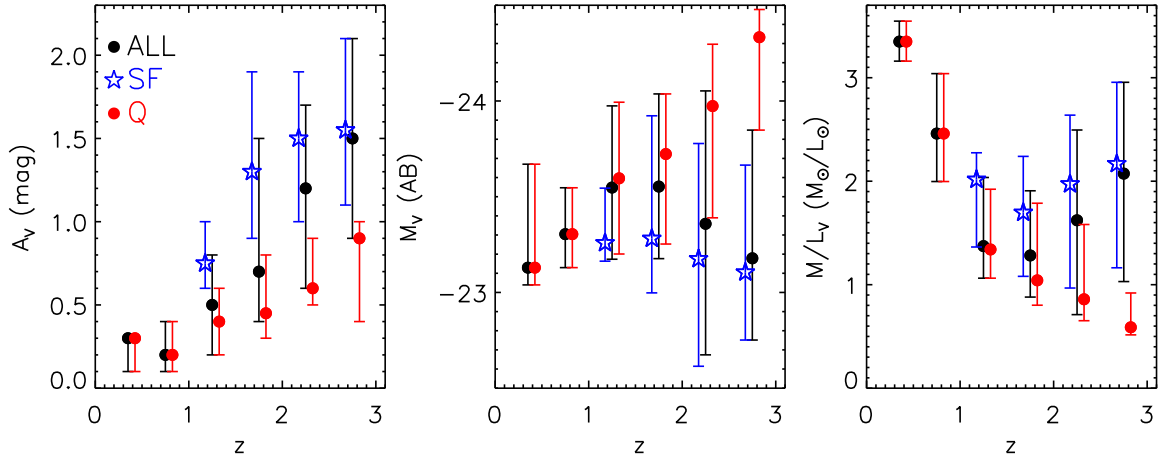


FIG. A14.— Evolution with redshift of the dust extinction (left), the rest-frame V -band absolute magnitude (middle), and the mass-to-light ratio in the rest-frame V -band, M_{star}/L_V , (right) for the progenitors of UMGs selected with the fixed cumulative number density approach. Symbols as in Figure 6.

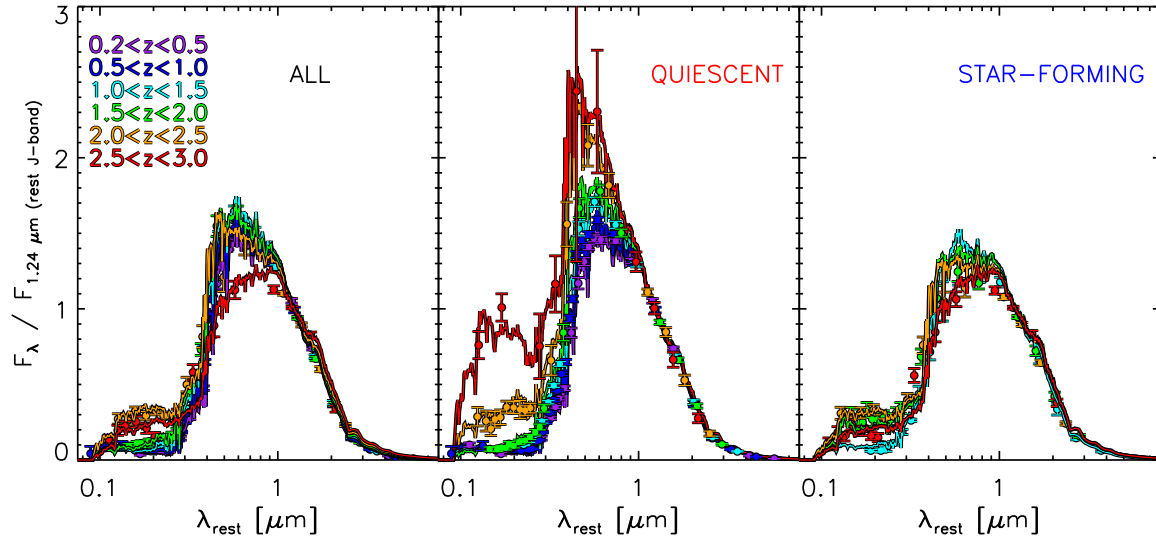


FIG. A15.— Evolution with redshift of the median rest-frame SEDs of the progenitors of UMGs selected with the fixed cumulative number density approach. Symbols as in Figure 7.

- Kim, D., & Im, M. 2013, *ApJ*, 766, 109
Kroupa, P. 2001, *MNRAS*, 322, 231
Kriek, M., et al. 2007, *ApJ*, 669, 776
Kriek, M., & Conroy, C. 2013, *ApJ*, 775, L16
Labbé, I., Bouwens, R., Illingworth, G. D., & Franx, M. 2006, *ApJ*, 649, L67
Labbé, I., et al. 2013, *ApJ*, 777, L19
Lagos, C., Bayet, E., Baugh, C. M., Lacey, C. G., Bell, T. A., Fanidakis, N., Geach, J. E. 2012, *MNRAS*, 426, 2142
Lapi, A., Raimundo, S., Aversa, R., Cai, Z.-Y., Negrello, M., Celotti, A., De Zotti, G., Danese, L. 2014, *ApJ*, 782, 69
Leitner, S. N. 2012, *ApJ*, 745, 149
Leja, J., van Dokkum, P., & Franx, M. 2013, *ApJ*, 766, 33
Lidman, C., et al. 2012, *MNRAS*, 427, 550
Lin, Y.-T., Brodwin, M., Gonzalez, A. H., Bode, P., Eisenhardt, P. R. M., Stanford, S. A., & Vikhlinin, A. 2013, *ApJ*, 771, 61
Lu, Y., Mo, H. J., Katz, N., & Weinberg, M. D. 2012, *MNRAS*, 421, 1779
Lu, Z., Mo, H., Lu, Y., Katz, N., Weinberg, M. D., van den Bosch, F. C., & Yang, X. 2014, *MNRAS*, 439, 1294
Malin, D. F., & Carter, D. 1983, *ApJ*, 274, 534
Marchesini, D. et al. 2009, *ApJ*, 701, 1765
Marchesini, D. et al. 2010, *ApJ*, 725, 1277
Marchesini, D., Stefanon, M., Brammer, G., & Whitaker, K. E. 2012, *ApJ*, 748, 126
Martin, D. C., et al. 2005, *ApJ*, 619, L1
McCracken, H. J., et al. 2012, *A&A*, 544, A156
McIntosh, D. H., Zabludoff, A. I., Rix, H.-W., & Caldwell, N. 2005, *ApJ*, 619, 193
Mei, S., et al. 2009, *ApJ*, 690, 42
Moster, B. P., Naab, T., & White, S. D. M. 2013, *MNRAS*, 428, 3121
Murphy, E. J., Chary, R.-R., Alexander, D. M., Dickinson, M., Magnelli, B., Morrison, G., Pope, A., & Teplitz, H. I. 2009, *ApJ*, 698, 1380
Mutch, S. J., Croton, D. J., & Poole, G. B. 2013, *MNRAS*, 435, 2445
Muzzin, A., Marchesini, D., van Dokkum, P. G., Labbé, I., Kriek, M., & Franx, M. 2009, *ApJ*, 701, 1839
Muzzin, A., van Dokkum, P. G., Kriek, M., Labbé, I., Cury, I., Marchesini, D., & Franx, M. 2010, *ApJ*, 725, 742
Muzzin, A., et al. 2013a, *ApJS*, 206, 8
Muzzin, A., et al. 2013b, *ApJ*, 777, 18
Nelán, J. E., et al. 2005, *ApJ*, 632, 137
Noll, S., Burgarella, D., Giovannoli, E., et al. 2009, *A&A*, 507, 1793
Papovich, C., et al. 2006, *ApJ*, 640, 92
Papovich, C., et al. 2007, *ApJ*, 668, 45
Papovich, C., Finkelstein, S. L., Ferguson, H. C., Lotz, J. M., & Giavalisco, M. 2011, *MNRAS*, 412, 1123
Patel, S. G., Kelson, D. D., Holden, B. P., Franx, M., & Illingworth, G. D. 2011, *ApJ*, 735, 53
Patel, S. G., Holden, B. P., Kelson, D. D., et al. 2012, *ApJ*, 748, L27
Patel, S. G., et al. 2013, *ApJ*, 766, 15
Pérez-González, P. G., et al. 2008, *ApJ*, 675, 234
Renzini, A. 2006, *ARA&A*, 44, 141
Rudnick, G., Rix, H.-W., Franx, M., et al. 2003, *ApJ*, 599, 847
Ruhland, C., Bell, E. F., Häubler, B., Taylor, E. N., Barden, M., & McIntosh, D. H. 2009, *ApJ*, 695, 1058
Sanders, D. B., et al. 2007, *ApJS*, 172, 86
Sheen, Y.-K., Yi, S. K., Ree, C. H., Lee, J. 2012, *ApJS*, 202, 8
Stark, D. P., et al. 2013, *ApJ*, 763, 129
Tal, T., van Dokkum, P. G., Nelán, J., Bezanson, R. 2009, *AJ*, 138, 1417
Thomas, D., Maraston, C., Bender, R., & Mendes de Oliveira, C. 2005, *ApJ*, 621, 673
Thomas, D., Maraston, C., Schawinski, K., Sarzi, M., & Silk, J. 2010, *MNRAS*, 404, 1775
Tojeiro, R., & Percival, W. J. 2010, *MNRAS*, 405, 2534
Tojeiro, R., et al. 2012, *MNRAS*, 424, 136
van Dokkum, P. G., Franx, M., Fabricant, D., Illingworth, G. D., & Kelson, D. D. 2000, *ApJ*, 541, 95
van Dokkum, P. G. 2005, *AJ*, 130, 2647
van Dokkum, P. G., & van der Marel, R. P. 2007, *ApJ*, 655, 30
van Dokkum, P. G. 2008, *ApJ*, 674, 29
van Dokkum, P. G., et al. 2013, *ApJ*, 771, L35
Vega, O., Silva, L., Panuzzo, P., Bressan, A., Granato, G. L., Chavez, M. 2005, *MNRAS*, 364, 1286
Wake, D. A., et al. 2006, *MNRAS*, 372, 537
Wang, L., et al. 2013, *MNRAS*, 431, 648
Webb, T. M. A., et al. 2006, *ApJ*, 636, L17
Whitaker, K. E., et al. 2010, *ApJ*, 719, 1715
Whitaker, K. E., et al. 2011, *ApJ*, 735, 86
Whitaker, K. E., et al. 2013, *ApJ*, 770, L39
Williams, R. J., Quadri, R. F., Franx, M., van Dokkum, P., & Labbé, I. 2009, *ApJ*, 691, 1879
Wuyts, S., et al. 2007, *ApJ*, 655, 51
Wuyts, S., et al. 2008, *ApJ*, 682, 985